RETHINKING GLOBAL TEXT CONDITIONING IN DIFFUSION TRANSFORMERS

Nikita Starodubcev[1*] **Daniil Pakhomov**[2] **Zongze Wu**[2] **Ilya Drobyshevskiy**[1]
Yuchen Liu[2] **Zhonghao Wang**[2] **Yuqian Zhou**[2] **Zhe Lin**[2] **Dmitry Baranchuk**[1]

[1]Yandex Research, [2]Adobe Research
https://github.com/quickjkee/modulation-guidance

ABSTRACT

Diffusion transformers typically incorporate textual information via (i) attention layers and (ii) a modulation mechanism using a pooled text embedding. Nevertheless, recent approaches discard modulation-based text conditioning and rely exclusively on attention. In this paper, we address **whether modulation-based text conditioning is necessary and whether it can provide any performance advantage**. Our analysis shows that, in its conventional usage, the pooled embedding contributes little to overall performance, suggesting that attention alone is generally sufficient for faithfully propagating prompt information. However, we reveal that the pooled embedding can provide significant gains when used from a different perspective—serving as guidance and enabling controllable shifts toward more desirable properties. This approach is training-free, simple to implement, incurs negligible runtime overhead, and can be applied to various diffusion models, bringing improvements across diverse tasks, including text-to-image/video generation and image editing.

1 INTRODUCTION

Since the pioneering works on diffusion models (DMs) (Ho et al., 2020; Song et al., 2020), the UNet architecture (Ronneberger et al., 2015) has served as the dominant backbone for diffusion-based image generation. This trend extended to text-to-image models (Saharia et al., 2022; Nichol et al., 2021), which employ UNet-based architectures (Rombach et al., 2022) and incorporate the CLIP text encoder (Radford et al., 2021) to condition the model on text sequences through the attention mechanism (Vaswani et al., 2017). Later, models such as Podell et al. (2023) began to incorporate the pooled CLIP embedding via modulation mechanisms (Karras et al., 2017; 2019), in addition to the token-wise text embeddings. More recently, works including Labs et al. (2025); Labs (2024); Esser et al. (2024); Kong et al. (2024); Cai et al. (2025) have adopted transformer-based architectures (Peebles & Xie, 2023) while retaining modulation-based text conditioning. Recent models (Wan et al., 2025; Wu et al., 2025; Agarwal et al., 2025; Xie et al., 2024) discard global text conditioning, achieving comparable text alignment by relying solely on attention. This transition raises questions about the role and necessity of global text conditioning, which we aim to explore.

We observe that, at first glance, modulation-based text conditioning appears non-contributory, and attention alone is sufficient to capture textual information. However, we argue that it is premature to discard global text conditioning and that it should instead be leveraged from a different perspective. Specifically, we draw inspiration from the interpretability of the modulation mechanism (Karras et al., 2019) and the ability of CLIP to control it (Garibi et al., 2025). We suggest that the pooled text embedding can act as a corrector, adjusting the diffusion trajectory toward better modes.

In summary, our contributions are as follows: **(1)** We conduct an in-depth analysis of global text conditioning in contemporary DMs and find that it plays only a minor role relative to attention-based text conditioning. **(2)** We show that global text conditioning can yield significant improvements when viewed from the perspective of *modulation guidance*. Furthermore, we enhance its effectiveness by proposing dynamic strategies. **(3)** We introduce techniques for integrating the pooled embedding

[*]Work partially done during an internship at Adobe Research

into fully attention-based models, thereby improving their performance via modulation guidance. **(4)** From a practical standpoint, our approach is simple to implement, incurs negligible overhead, and delivers performance gains on state-of-the-art multi- and few-step DMs across text-to-image/video and image-editing tasks.

2 RELATED WORK

Several post-training approaches have been proposed to improve DM quality. The first group centers on *classifier-free guidance (CFG) modifications* (Ho & Salimans, 2022). Specifically, prior works improve CFG by optimizing scale factors (Fan et al., 2025), addressing off-manifold challenges (Chung et al., 2024), modifying the unconditional branch (Karras et al., 2024), mitigating oversaturation at high CFG scales (Sadat et al., 2024; 2025; Lin et al., 2024), and introducing dynamic CFG strategies (Kynkäänniemi et al., 2024; Sadat et al., 2023; Wang et al., 2024; Yehezkel et al., 2025). In contrast, our method complements CFG and, importantly, can also be applied to few-step DMs (Song et al., 2023; Sauer et al., 2024b; Yin et al., 2024a; Starodubcev et al., 2025) that do not use CFG.

The second group focuses on *test-time optimization*. A dominant line of work (Chefer et al., 2023; Seo et al., 2025; Yiflach et al., 2025; Li et al., 2023; Rassin et al., 2023; Agarwal et al., 2023; Dahary et al., 2024; Marioriyad et al., 2025; Binyamin et al., 2025; Phung et al., 2024; Chen et al., 2024; Kwon et al., 2022) relies on handcrafted loss functions, typically guided by heuristics about how attention maps should behave, and optimizes these maps accordingly. Other methods focus on optimizing only the initial noise rather than the full denoising trajectory (Eyring et al., 2025; Ma et al., 2025a; Eyring et al., 2024; Guo et al., 2024), or on fine-tuning LoRAs to extract different concepts (Gandikota et al., 2024). In contrast, our approach avoids complex loss design and intensive model tuning while still improving performance.

Finally, works most closely related to ours are *attention guidance methods*. These methods (Chen et al., 2025; Hong et al., 2023; Ahn et al., 2025; Nguyen et al., 2024) leverage positive and negative prompts, compute attention outputs for both, and perform controlled extrapolation in the attention space—pushing the model toward positive prompts and away from negative ones. Our approach also relies on guidance in feature space but applies it through a small MLP rather than through attention.

3 MODULATION LAYERS

In this section, we briefly recap the key components of modulation layers used in transformer DMs.

State-of-the-art text-to-image DMs (Labs, 2024; Cai et al., 2025) typically represent images as sequences of continuous tokens, aligning them with text tokens in a unified representation. This combined sequence is processed through a series of transformer blocks (Peebles & Xie, 2023), which primarily consist of MLPs, normalization, and attention layers. To condition the model on a text prompt, two types of encoders are usually used: a $\mathrm{T5}$ (Raffel et al., 2020) and a CLIP text encoder (Radford et al., 2021), which operate as follows:

$$\mathbf{y}(\mathbf{p}, t) = \mathrm{MLP}\big(t,\ \mathrm{CLIP}(\mathbf{p})\big), \quad \mathbf{s} = \big[\mathrm{T5}(\mathbf{p}),\ \mathbf{x}\big], \tag{1}$$

Here, $\mathbf{y}$ denotes a global conditioning vector derived from the time step t and the pooled embedding of the prompt $\mathbf{p}$, whereas $\mathbf{s}$ denotes the concatenated sequence of image tokens $\mathbf{x}$ and text tokens $\mathrm{T5}(\mathbf{p})$. The sequence $\mathbf{s}$ is then processed via cross-attention to incorporate text information, while the global conditioning vector $\mathbf{y}$ is shared across the entire model and constructs a modulation space that influences the modulation layers.

$$\mathrm{Mod}(\mathbf{s},\ \mathbf{y}) = \alpha_{\mathbf{s}}(\mathbf{y}) \cdot \mathbf{s} + \beta_{\mathbf{s}}(\mathbf{y}), \tag{2}$$

Here, $\alpha_{\mathbf{s}}$ and $\beta_{\mathbf{s}}$ are the coefficients of the modulation layer, representing scaling and shifting operations, respectively. Notably, modulation layers have proved effective in enabling semantic control and transformation in GANs (Karras et al., 2019; 2020; 2021). In DMs, they have been used to address image editing problems (Garibi et al., 2025; Dalva et al., 2024). While these layers have shown effectiveness in semantic control tasks, their role in improving image generation quality remains unexplored.

Configuration		CLIP Score ↑	PickScore ↑	ImageReward ↑
FLUX schnell				
Initial,	short	30.1	21.6	6.2
w/o CLIP,	short	29.0 (−1.1)	21.3 (−0.3)	4.5 (−1.7)
w/o T5,	short	28.9 (−1.2)	21.0 (−0.6)	1.5 (−4.7)
Initial,	long	33.1	21.0	10.3
w/o CLIP,	long	32.8 (−0.3)	21.0 (−0.0)	10.4 (+0.1)
w/o T5,	long	30.7 (−2.4)	19.9 (−1.1)	2.4 (−7.9)
HiDream-Fast				
Initial,	short	30.3	21.8	7.9
w/o CLIP,	short	30.3 (−0.0)	21.8 (−0.0)	8.1 (+0.1)
w/o Llama,	short	20.2 (−10.1)	18.2 (−3.6)	−21.5 (−29.4)
Initial,	long	32.9	21.5	12.8
w/o CLIP,	long	32.9 (−0.0)	21.5 (−0.0)	13.0 (+0.2)
w/o Llama,	long	16.8 (−16.1)	16.0 (−4.5)	−20.8 (−33.6)

Table 1: Image quality results for short and long prompts. The CLIP embedding does not affect output quality on long prompts for **FLUX schnell** and has no effect for **HiDream-Fast**.

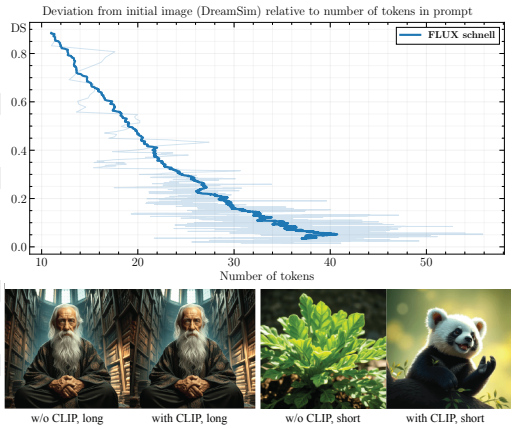

Figure 1: **(top)** Difference between images (DreamSim) with and without CLIP as a function of prompt length. **(bot)** For long prompts, images without CLIP generally do not differ from the initial ones.

4 Analysis of the Pooled Text Embedding Role

In recent DMs, there is a trend to discard the pooled text embedding and rely solely on the timestep t to produce $\mathbf{y}$, i.e., $\mathrm{MLP}\big(t,\ \mathrm{CLIP}(\mathbf{p})\big) \rightarrow \mathrm{MLP}\big(t\big)$. In this setup, the text is incorporated only through the text encoder T5. However, no strict justification for this design choice has been provided. Therefore, in this section, we investigate the impact of the pooled embedding on the generative performance of DMs.

Influence of the CLIP pooled embedding. First, we analyze the influence of CLIP on text-to-image generation performance. To this end, we examine two contemporary models: FLUX schnell and HiDream-Fast. Specifically, we analyze the impact of CLIP by removing the pooled embedding, setting $\mathrm{CLIP}(\mathbf{p}) \rightarrow 0$, and comparing it to the standard case with CLIP enabled. Our key observation is that **the pooled CLIP embedding is partially inactive in FLUX schnell and fully inactive in HiDream-Fast**.

Specifically, we find that the influence of CLIP in **FLUX schnell** is inconsistent: it is negligible for long prompts but can be impactful for short ones. To confirm this, we construct two subsets of prompts (1K each) from the MJHQ dataset (Li et al., 2024): short (10 tokens) and long (77 tokens). We then evaluate the DM's performance on each subset. In Table 1 (top), we report image quality metrics (CLIP Score, PickScore, and ImageReward) for each subset. We observe that for long prompts, CLIP has little effect, with only a minimal impact on quality. In contrast, for short prompts, its influence is more pronounced.

Moreover, in Figure 1, we analyze the difference between images generated with and without CLIP as a function of prompt length (measured by the number of tokens). We find that for longer prompts, the deviation from the initial generation becomes negligible, and the images fully resemble the initial ones, as visually confirmed in Figure 1 (bottom).

For **HiDream-Fast**, we observe slightly different behavior: the CLIP pooled embedding exhibits no effect for either short or long prompts, as numerically confirmed in Table 1 (bottom).

Influence of the pooled embedding on other models. Additionally, we explore the reintegration of CLIP into a DM from which it was originally absent. To this end, we consider the COSMOS model (Agarwal et al., 2025) and incorporate the CLIP pooled embedding into it as described in Section 5. In this case, we observe the same behavior as with the HiDream-Fast model: CLIP has no influence. This result is numerically confirmed in Section 6. Finally, in Appendix A, we observe the same effect in the instruction-guided image editing task performed with the FLUX Kontext model. In Section 6, we show that this limitation can result in insufficient editing strength for complex cases.

5 MODULATION GUIDANCE

Our observations raise questions about the necessity of using the pooled embedding in generative tasks. **However, although the pooled text embedding may seem uninformative in some cases, we propose reconsidering its role from a different perspective—one that can lead to improved generative performance in DMs.**

Guidance in modulation space. We draw inspiration from the understanding that modulation layers can drive semantic changes in generated images (Karras et al., 2019). Moreover, the CLIP encoder is trained to construct a shared space between images and text, resulting in interpretable geometry. Thus, we suggest that CLIP enables interpretable modifications of the modulation space using natural language and guides the model toward modes with more desirable properties.

We propose a training-free, plug-and-play technique to reactivate CLIP and strengthen its influence during generation, drawing inspiration from Garibi et al. (2025). Specifically, we amplify its effect by introducing guidance in the modulation space.

$$\mathbf{y}(\mathbf{p}, t) \rightarrow \hat{\mathbf{y}}(\mathbf{p}, \mathbf{p}_+, \mathbf{p}_-, t) = \mathbf{y}(\mathbf{p}, t) + w \cdot \big(\mathbf{y}(\mathbf{p}_+, t) - \mathbf{y}(\mathbf{p}_-, t)\big). \tag{3}$$

We note that $\hat{\mathbf{y}}$ affects only the modulation coefficients and is shared across all DM blocks, thereby incurring negligible computational overhead compared to basic generation. Moreover, this technique can be applied on top of CFG guidance or with distilled DMs that do not rely on CFG.

To provide intuition behind the guidance, we first analyze it from the perspective of semantic changes. Prior work has focused on identifying interpretable directions in DMs, either through supervised (Gandikota et al., 2024) or unsupervised approaches (Gandikota et al., 2025). In contrast, we demonstrate that such interpretable directions are already embedded within the model and can be accessed by shifting in the modulation space. Specifically, in Figure 2, we consider two examples: $\mathbf{p}_+$ = `Long hair; Modern car` and $\mathbf{p}_-$ = `Short hair; Old car`. We observe that the pooled embedding can substantially influence the generated image, leading to both local (hair length) and global (car style) changes.

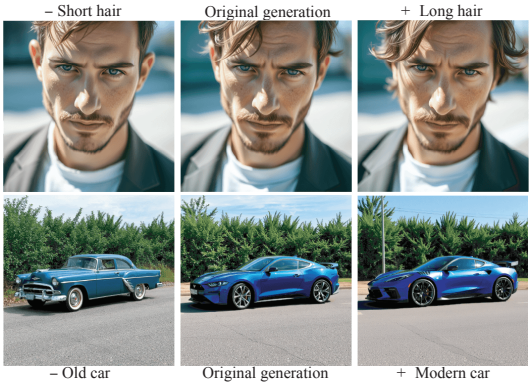

Figure 2: The modulation guidance enables local (top) and global (bottom) changes and encourages its use to shift a DM toward modes with better properties.

Our observations suggest that modulation guidance provides an additional degree of freedom in generation, beyond what CFG offers. Building on this, we propose using it to enhance generation quality across multiple dimensions. Specifically, we consider **general changes:** `aesthetics, complexity`, and **specific changes:** `hands correction, object counting, color, position`. For the latter, we focus on common criteria typically measured in T2I benchmarks (Ghosh et al., 2023). Notably, our technique requires only the selection of a suitable prompt for each category—no additional training or fine-tuning is necessary. In Appendix D, we present the prompts used for each targeted aspect.

Dynamic modulation guidance. We find that a constant guidance scale w is generally effective, but excessively high values can overweight the prompt and cause the model to neglect textual information (Appendix C). To address this, we draw inspiration from dynamic CFG (Sadat et al., 2023; Kynkäänniemi et al., 2024), which has shown promising results in DMs. Unlike dynamic CFG, we aim to adjust w across layers rather than across time steps.

We consider the simplest variant present in Figure 3(b). We discuss more strategies in Appendix B. First, we compare the dynamic version against constant modulation guidance in terms of the aesthetics–prompt fidelity trade-off. To this end, we apply both types of guidance with different scales w on 1K prompts from the MJHQ dataset (Lian et al., 2023). We compute PickScore (Kirstain et al., 2023) for aesthetics quality and CLIP score (Hessel et al., 2021) for text correspondence. The results presented in Figure 3(a) confirm that dynamic guidance provides a better trade-off than constant

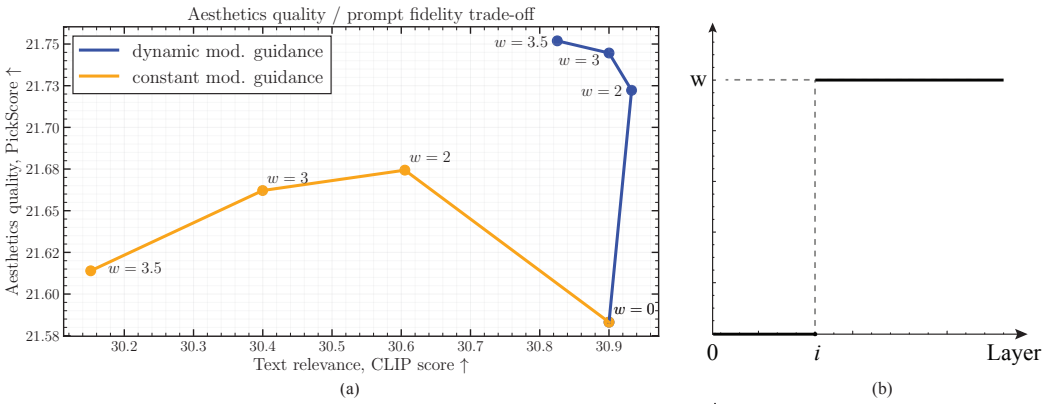

Figure 3: **Analysis on dynamic modulation guidance.** (a) Dynamic guidance offers a better trade-off between aesthetic quality and prompt correspondence than constant modulation guidance. (b) We use a step function, controlled by i, that skips the first few layers of the model as our form of dynamic guidance. Additional variants are explored in Appendix B.

guidance. Our approach improves image quality without compromising prompt correspondence relative to $w = 0$ (the initial model without modulation guidance).

In our experiments, we find that dynamic modulation guidance generalizes well across tasks, suggesting that it can be applied to new tasks without additional tuning. We also observe that more complex strategies (Appendix C) can yield better results in some cases, offering an additional degree of improvement.

What does modulation guidance actually do? We address the question of how the model is affected by the guidance in improving the generated content. To this end, we analyze the case of `hands correction`. Specifically, in Figure 4(a), we visualize the attention map corresponding to the word `hands` for a specific image. Interestingly, we observe that the model places greater focus on the relevant region, highlighting it more distinctly. In addition, in Figure 4(b, left), we plot the averaged attention map for all tokens in the corresponding prompt. We find that the model primarily shifts its attention toward more relevant tokens—such as `hands` and `child`.

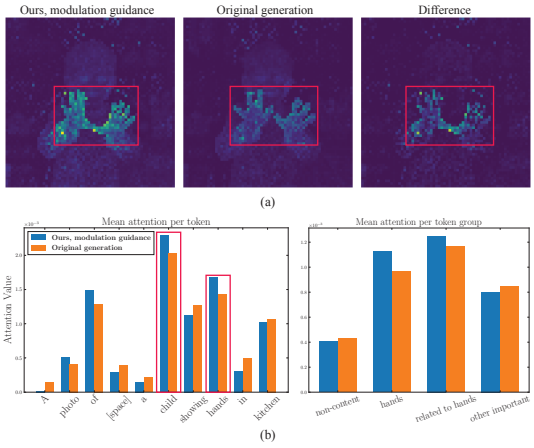

Figure 4: After applying modulation guidance, the model focuses more on the desired features, such as hands (a, b).

To confirm this intuition, we analyze a subset of prompts focused on `hands correction` and split all tokens into four groups: non-content tokens, the token `hands`, tokens related to hands, and other important tokens. The results in Figure 4(b, right) confirm that the model shifts its attention toward `hands` and hand-related tokens.

Integrating the pooled text embedding into CLIP-free models. Finally, we extend modulation guidance to models without pooled text embeddings, showing that it can improve generation quality. To this end, we fine-tune existing text-to-image/video models Agarwal et al. (2025); Wan et al. (2025) by introducing the pooled embedding. Specifically, we train a small MLP on top of the pooled text embedding and add it to the timestep embedding, while keeping the rest of the network frozen. The model behaves identically to the original when the pooled embedding is set to 0. Importantly, we train on the model's own synthetic data to ensure that improvements do not stem from dataset differences.

Table 2: Performance of text-to-image DMs with and without modulation guidance (gray) on Aesthetics and Complexity, evaluated with human preferences and automatic metrics. Human win rates are reported with respect to the original model; green indicates statistically significant improvement, red a decline. For automatic metrics, **bold** denotes improvement over the original model.

Model	Side-by-Side Win Rate, %				Automatic Metrics, COCO 5k			
	Relevance ↑	Aesthetics ↑	Complexity ↑	Defects ↑	PickScore ↑	CLIP ↑	IR ↑	HPSv3 ↑
FLUX schnell					22.9	35.6	10.2	11.3
Aesthetics	48	**72**	**78**	48	**23.1**	**35.8**	**11.0**	**11.8**
Complexity	53	**56**	**69**	47	**23.0**	**35.9**	**10.8**	**11.4**
FLUX dev					23.1	34.7	10.5	12.4
Aesthetics	44	**56**	**69**	52	**23.2**	34.5	**11.0**	**12.8**
Complexity	48	**59**	**72**	47	23.1	34.6	**11.1**	**12.8**
SD3.5 Large					23.0	35.8	10.5	11.1
Aesthetics	50	**62**	**70**	47	**23.1**	**35.9**	**10.7**	**11.2**
Complexity	49	49	**60**	45	23.0	35.8	**11.7**	11.0
HiDream					23.4	34.4	11.7	13.2
Aesthetics	49	**60**	**80**	46	**23.5**	34.4	**12.1**	**13.7**
Complexity	47	52	**70**	45	**23.5**	34.4	**11.9**	**13.3**
COSMOS					23.0	35.0	11.4	12.3
+ CLIP	50	49	43	50	23.0	35.0	11.4	12.2
Aesthetics	50	**60**	**70**	45	**23.2**	35.0	**11.7**	**12.6**
Complexity	50	52	**61**	44	23.0	**35.4**	**11.8**	**12.4**

We highlight two important aspects of the training process. First, we propagate the textual prompt solely through the pooled text embedding, using an unconditional prompt for T5. This design forces the model to perceive textual information through the pooled embedding. Second, we employ a distillation-based training regime. Specifically, we sample a clean image, add noise to it, and then generate two predictions: one from the original model (without the pooled embedding) and one from the modified model (with the pooled embedding). The objective is to minimize the MSE loss between these two predictions. This distillation approach is well-suited for few-step DMs, as it eliminates the need for complex adversarial or distribution-matching losses (Yin et al., 2024a).

6 Experiments

6.1 Text-to-Image Generation

Configuration. We validate our approach on state-of-the-art text-to-image DMs that include modulation-based text conditioning: FLUX schnell (Sauer et al., 2024a), FLUX (Labs, 2024), SD3.5 Large (Esser et al., 2024), and HiDream (Cai et al., 2025). In addition, we consider the CLIP-free COSMOS model (Agarwal et al., 2025) and fine-tune it for 4K iterations to introduce the pooled text embedding. We train the model on its own synthetic dataset of 500K samples, following the generation settings of Agarwal et al. (2025) and using prompts from Li et al. (2024).

We evaluate performance using two types of metrics: human preference and automatic evaluation. Human preference is measured via side-by-side comparisons, where annotators assess image pairs on four criteria: text relevance, aesthetics, complexity, and defects (details in Appendix J). For general changes, we use 128 prompts from PartiPrompts (Yu et al., 2022), generating two images per prompt. For specific changes, we use 70 prompts from CompBench (Jia et al., 2025) for `object counting` and 200 LLM-generated prompts for `hands correction`. For automatic evaluation, we report CLIP score (Hessel et al., 2021), ImageReward (IR) (Xu et al., 2023), PickScore (PS) (Kirstain et al., 2023), and HPSv3 (Ma et al., 2025b), tested on 5K prompts from COCO2014 (Lin et al., 2014). We also use GenEval (Ghosh et al., 2023) to validate modulation guidance across multiple benchmark criteria.

Our main baselines are the original models without modulation guidance. In addition, we consider the Normalized Attention Guidance approach (Chen et al., 2025) and LLM-enhanced prompt modifiers (Lian et al., 2023). Finally, we include the test-time optimization method Concept Sliders (Gandikota et al., 2024) for the `hands correction` task.

Figure 5: Qualitative results of modulation guidance for `Aesthetics` (top) and `Complexity` (bottom). The `Aesthetics` guidance notably improves image quality, while the `Complexity` guidance can enhance the complexity of both the main object and background details.

General changes. In this case, we focus on two aspects for improvement: `aesthetics` and `complexity`. These aspects are crucial for text-to-image generation and are typically the targets of self-supervised fine-tuning techniques (Startsev et al., 2025) or RL-based approaches (Wallace et al., 2024), which are commonly adopted in DMs. However, we demonstrate that our simple technique achieves significant improvements without any fine-tuning. The only requirement is to select appropriate positive and negative prompts, along with a suitable dynamic guidance strategy. Our choices are summarized in Table 5 and discussed in Appendix D.

Table 2 reports numerical results, showing clear human preference gains for both aspects. `Aesthetics` guidance significantly improves both aesthetics and complexity, while `complexity` guidance mainly enhances complexity. Automatic metrics show consistent ImageReward gains across all models and HPSv3 improvements in most cases, except for SD3.5 Large with `complexity` guidance. Importantly, we observe that introducing CLIP into COSMOS does not improve performance and even reduces complexity; gains appear only when combined with modulation guidance, confirming that CLIP alone is ineffective. We note slight drops in text relevance for FLUX dev and in defects for COSMOS, though these are minor. Qualitative examples are shown in Figure 5 and Appendix I.

Specific changes. Next, we focus on improving `object counting`, `hands correction`, `color`, and `position`. The first two are particularly important, as they have been extensively studied in prior work (Binyamin et al., 2025; Gandikota et al., 2024). For `object counting`, we use the number of target objects as the positive direction, while for `hands correction`, we draw

Table 3: Quantitative results of the modulation guidance for specific changes. The modulation guidance yields improvements according to GenEval and human preference.

Model		GenEval			SbS Win Rate, %	
		Object Counting	Color	Position	Object Counting	Hands correction
FLUX schnell	Original	56	79	25	39	41
	Ours	65 (+9)	86 (+7)	30 (+5)	61 (+22)	59 (+18)

Figure 6: Qualitative results of the modulation guidance for `Object counting` (top) and `Hands correction` (bottom).

inspiration from Gandikota et al. (2024) in designing positive and negative prompts. Further details are provided in Table 5.

We present the results in Table 3 and Figure 6. Improvements are observed in several aspects of the GenEval benchmark, including object counting, color, and position. According to human evaluation, our approach improves the original model by 22% in `object counting` and 18% in `hands correction`. We report text relevance and defects as the evaluation criteria for object counting and hands correction, respectively.

Comparison with baselines. Normalized Attention Guidance (Chen et al., 2025) targets general changes, so we compare it with our `aesthetics` guidance using SbS evaluation. Similarly, we compare Concept Sliders (Gandikota et al., 2024) with our `hands correction` guidance by evaluating defects. For LLM-enhanced prompts (Lian et al., 2023), we consider general changes, `hands correction`, and `object counting`. Results in Appendix E (Tables 8 and 9) show that our approach outperforms Normalized Attention Guidance by 34% and Concept Sliders by 16%, without additional computational overhead. Moreover, Table 8 shows that modulation guidance can further improve performance when combined with LLM-enhanced prompts.

Table 4: Quantative evaluation on VBench. The results show an improved dynamic degree compared to the original models and baseline approach (normalized attention guidance).

Model, video		total score ↑	motion smoothness ↑	dynamic degree ↑	aesthetic quality ↑	overall consistency ↑
Hunyan, 13B	Original	56.68	**99.23**	50.51	55.88	21.08
	Modulation guidance	**57.56**	99.03	**53.61**	**56.50**	**21.09**
CausVid, 1.3B	Original	62.72	**98.76**	75.25	57.85	19.01
	+ CLIP	62.82	98.63	76.38	57.77	18.49
	Norm. attent. guidance	63.58	98.39	74.22	**62.08**	**19.61**
	Modulation guidance	**65.43**	98.45	**86.59**	57.65	19.02

Figure 7: Qualitative comparison between the original CausVid and CausVid with modulation guidance.

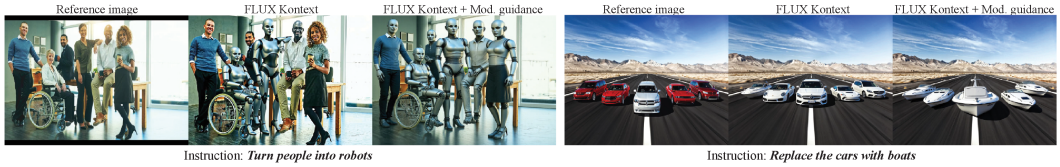

Figure 8: Qualitative results for text-guided image editing tasks. We observe that FLUX Kontext sometimes struggles with complex edits, while modulation guidance can mitigate this limitation.

6.2 Text-to-video Generation

Configuration. We apply modulation guidance to Hunyuan 13B (Kong et al., 2024) and CausVid 1.3B (Yin et al., 2024b). The latter does not include a CLIP model, so we fine-tune it for 1K iterations. To evaluate performance, we use VBench (Huang et al., 2024), which covers various aspects. In this experiment, we apply the same `aesthetics` guidance as in the text-to-image task. In addition, we compare our approach with Normalized Attention Guidance.

Results. The results are presented in Table 4 and Figure 7. Importantly, we observe improvements in dynamic degree for both models, with particularly strong gains for CausVid. This is notable because CausVid is distilled from WAN (Wan et al., 2025), and video models typically lose dynamics after distillation. Furthermore, we find that incorporating CLIP provides no improvement. Additional visual comparisons are provided in Appendix I.

6.3 Instruction-guided Image Editing

Finally, we address image editing using the FLUX Kontext model (Labs et al., 2025), which, as we find, can struggle with complex edits involving multiple objects. To overcome this, we apply modulation guidance, using the final prompt as the positive direction and a blank prompt as the negative. We validate our approach on the SEED-Data benchmark (Ge et al., 2024) and present the results and implementation details in Appendix F. Representative examples are shown in Figure 8.

7 Conclusion

In this paper, we revisit the role of the pooled text embedding, showing that, despite its weak influence, it can improve performance across tasks and models when used from a different perspective. We present ablation studies in Appendix C, where dynamic modulation guidance outperforms constant guidance, offering greater flexibility for practitioners. Limitations are discussed in Appendix H.

REFERENCES

Aishwarya Agarwal, Srikrishna Karanam, KJ Joseph, Apoorv Saxena, Koustava Goswami, and Balaji Vasan Srinivasan. A-star: Test-time attention segregation and retention for text-to-image synthesis. In *Proceedings of the IEEE/CVF International Conference on Computer Vision*, pp. 2283–2293, 2023.

Niket Agarwal, Arslan Ali, Maciej Bala, Yogesh Balaji, Erik Barker, Tiffany Cai, Prithvijit Chattopadhyay, Yongxin Chen, Yin Cui, Yifan Ding, et al. Cosmos world foundation model platform for physical ai. *arXiv preprint arXiv:2501.03575*, 2025.

Donghoon Ahn, Hyoungwon Cho, Jaewon Min, Wooseok Jang, Jungwoo Kim, SeonHwa Kim, Hyun Hee Park, Kyong Hwan Jin, and Seungryong Kim. Self-rectifying diffusion sampling with perturbed-attention guidance, 2025. URL https://arxiv.org/abs/2403.17377.

Omri Avrahami, Or Patashnik, Ohad Fried, Egor Nemchinov, Kfir Aberman, Dani Lischinski, and Daniel Cohen-Or. Stable flow: Vital layers for training-free image editing. In *Proceedings of the Computer Vision and Pattern Recognition Conference*, pp. 7877–7888, 2025.

Shuai Bai, Keqin Chen, Xuejing Liu, Jialin Wang, Wenbin Ge, Sibo Song, Kai Dang, Peng Wang, Shijie Wang, Jun Tang, Humen Zhong, Yuanzhi Zhu, Mingkun Yang, Zhaohai Li, Jianqiang Wan, Pengfei Wang, Wei Ding, Zheren Fu, Yiheng Xu, Jiabo Ye, Xi Zhang, Tianbao Xie, Zesen Cheng, Hang Zhang, Zhibo Yang, Haiyang Xu, and Junyang Lin. Qwen2.5-vl technical report. *arXiv preprint arXiv:2502.13923*, 2025.

Lital Binyamin, Yoad Tewel, Hilit Segev, Eran Hirsch, Royi Rassin, and Gal Chechik. Make it count: Text-to-image generation with an accurate number of objects. In *Proceedings of the Computer Vision and Pattern Recognition Conference*, pp. 13242–13251, 2025.

Qi Cai, Jingwen Chen, Yang Chen, Yehao Li, Fuchen Long, Yingwei Pan, Zhaofan Qiu, Yiheng Zhang, Fengbin Gao, Peihan Xu, et al. Hidream-i1: A high-efficient image generative foundation model with sparse diffusion transformer. *arXiv preprint arXiv:2505.22705*, 2025.

Hila Chefer, Yuval Alaluf, Yael Vinker, Lior Wolf, and Daniel Cohen-Or. Attend-and-excite: Attention-based semantic guidance for text-to-image diffusion models. *ACM transactions on Graphics (TOG)*, 42(4):1–10, 2023.

Dar-Yen Chen, Hmrishav Bandyopadhyay, Kai Zou, and Yi-Zhe Song. Normalized attention guidance: Universal negative guidance for diffusion models, 2025. URL https://arxiv.org/abs/2505.21179.

Minghao Chen, Iro Laina, and Andrea Vedaldi. Training-free layout control with cross-attention guidance. In *Proceedings of the IEEE/CVF winter conference on applications of computer vision*, pp. 5343–5353, 2024.

Hyungjin Chung, Jeongsol Kim, Geon Yeong Park, Hyelin Nam, and Jong Chul Ye. Cfg++: Manifold-constrained classifier free guidance for diffusion models. *arXiv preprint arXiv:2406.08070*, 2024.

Omer Dahary, Or Patashnik, Kfir Aberman, and Daniel Cohen-Or. Be yourself: Bounded attention for multi-subject text-to-image generation, 2024. URL https://arxiv.org/abs/2403.16990.

Yusuf Dalva, Kavana Venkatesh, and Pinar Yanardag. Fluxspace: Disentangled semantic editing in rectified flow transformers, 2024. URL https://arxiv.org/abs/2412.09611.

Patrick Esser, Sumith Kulal, Andreas Blattmann, Rahim Entezari, Jonas Müller, Harry Saini, Yam Levi, Dominik Lorenz, Axel Sauer, Frederic Boesel, et al. Scaling rectified flow transformers for high-resolution image synthesis. In *Forty-first international conference on machine learning*, 2024.

Luca Eyring, Shyamgopal Karthik, Karsten Roth, Alexey Dosovitskiy, and Zeynep Akata. Reno: Enhancing one-step text-to-image models through reward-based noise optimization. *Neural Information Processing Systems (NeurIPS)*, 2024.

Luca Eyring, Shyamgopal Karthik, Alexey Dosovitskiy, Nataniel Ruiz, and Zeynep Akata. Noise hypernetworks: Amortizing test-time compute in diffusion models. *arXiv preprint arXiv:2508.09968*, 2025.

Weichen Fan, Amber Yijia Zheng, Raymond A Yeh, and Ziwei Liu. Cfg-zero*: Improved classifier-free guidance for flow matching models. *arXiv preprint arXiv:2503.18886*, 2025.

Rohit Gandikota, Joanna Materzyńska, Tingrui Zhou, Antonio Torralba, and David Bau. Concept sliders: Lora adaptors for precise control in diffusion models. In *European Conference on Computer Vision*, pp. 172–188. Springer, 2024.

Rohit Gandikota, Zongze Wu, Richard Zhang, David Bau, Eli Shechtman, and Nick Kolkin. Sliderspace: Decomposing the visual capabilities of diffusion models. *arXiv preprint arXiv:2502.01639*, 2025.

Daniel Garibi, Shahar Yadin, Roni Paiss, Omer Tov, Shiran Zada, Ariel Ephrat, Tomer Michaeli, Inbar Mosseri, and Tali Dekel. Tokenverse: Versatile multi-concept personalization in token modulation space, 2025. URL https://arxiv.org/abs/2501.12224.

Yuying Ge, Sijie Zhao, Chen Li, Yixiao Ge, and Ying Shan. Seed-data-edit technical report: A hybrid dataset for instructional image editing, 2024. URL https://arxiv.org/abs/2405.04007.

Dhruba Ghosh, Hannaneh Hajishirzi, and Ludwig Schmidt. Geneval: An object-focused framework for evaluating text-to-image alignment. *Advances in Neural Information Processing Systems*, 36: 52132–52152, 2023.

Xiefan Guo, Jinlin Liu, Miaomiao Cui, Jiankai Li, Hongyu Yang, and Di Huang. Initno: Boosting text-to-image diffusion models via initial noise optimization, 2024. URL https://arxiv.org/abs/2404.04650.

Jack Hessel, Ari Holtzman, Maxwell Forbes, Ronan Le Bras, and Yejin Choi. Clipscore: A reference-free evaluation metric for image captioning. *arXiv preprint arXiv:2104.08718*, 2021.

Jonathan Ho and Tim Salimans. Classifier-free diffusion guidance. *arXiv preprint arXiv:2207.12598*, 2022.

Jonathan Ho, Ajay Jain, and Pieter Abbeel. Denoising diffusion probabilistic models. *Advances in neural information processing systems*, 33:6840–6851, 2020.

Susung Hong, Gyuseong Lee, Wooseok Jang, and Seungryong Kim. Improving sample quality of diffusion models using self-attention guidance, 2023. URL https://arxiv.org/abs/2210.00939.

Ziqi Huang, Yinan He, Jiashuo Yu, Fan Zhang, Chenyang Si, Yuming Jiang, Yuanhan Zhang, Tianxing Wu, Qingyang Jin, Nattapol Chanpaisit, Yaohui Wang, Xinyuan Chen, Limin Wang, Dahua Lin, Yu Qiao, and Ziwei Liu. VBench: Comprehensive benchmark suite for video generative models. In *Proceedings of the IEEE/CVF Conference on Computer Vision and Pattern Recognition*, 2024.

Bohan Jia, Wenxuan Huang, Yuntian Tang, Junbo Qiao, Jincheng Liao, Shaosheng Cao, Fei Zhao, Zhaopeng Feng, Zhouhong Gu, Zhenfei Yin, Lei Bai, Wanli Ouyang, Lin Chen, Fei Zhao, Zihan Wang, Yuan Xie, and Shaohui Lin. Compbench: Benchmarking complex instruction-guided image editing, 2025. URL https://arxiv.org/abs/2505.12200.

Tero Karras, Timo Aila, Samuli Laine, and Jaakko Lehtinen. Progressive growing of gans for improved quality, stability, and variation. *arXiv preprint arXiv:1710.10196*, 2017.

Tero Karras, Samuli Laine, and Timo Aila. A style-based generator architecture for generative adversarial networks. In *Proceedings of the IEEE/CVF conference on computer vision and pattern recognition*, pp. 4401–4410, 2019.

Tero Karras, Miika Aittala, Janne Hellsten, Samuli Laine, Jaakko Lehtinen, and Timo Aila. Training generative adversarial networks with limited data. In *Proc. NeurIPS*, 2020.

Tero Karras, Miika Aittala, Samuli Laine, Erik Härkönen, Janne Hellsten, Jaakko Lehtinen, and Timo Aila. Alias-free generative adversarial networks. In *Proc. NeurIPS*, 2021.

Tero Karras, Miika Aittala, Tuomas Kynkäänniemi, Jaakko Lehtinen, Timo Aila, and Samuli Laine. Guiding a diffusion model with a bad version of itself. *Advances in Neural Information Processing Systems*, 37:52996–53021, 2024.

Yuval Kirstain, Adam Polyak, Uriel Singer, Shahbuland Matiana, Joe Penna, and Omer Levy. Pick-a-pic: An open dataset of user preferences for text-to-image generation. *Advances in neural information processing systems*, 36:36652–36663, 2023.

Weijie Kong, Qi Tian, Zijian Zhang, Rox Min, Zuozhuo Dai, Jin Zhou, Jiangfeng Xiong, Xin Li, Bo Wu, Jianwei Zhang, et al. Hunyuanvideo: A systematic framework for large video generative models. *arXiv preprint arXiv:2412.03603*, 2024.

Mingi Kwon, Jaeseok Jeong, and Youngjung Uh. Diffusion models already have a semantic latent space. *arXiv preprint arXiv:2210.10960*, 2022.

Tuomas Kynkäänniemi, Miika Aittala, Tero Karras, Samuli Laine, Timo Aila, and Jaakko Lehtinen. Applying guidance in a limited interval improves sample and distribution quality in diffusion models. *Advances in Neural Information Processing Systems*, 37:122458–122483, 2024.

Black Forest Labs. Flux. `https://github.com/black-forest-labs/flux`, 2024.

Black Forest Labs, Stephen Batifol, Andreas Blattmann, Frederic Boesel, Saksham Consul, Cyril Diagne, Tim Dockhorn, Jack English, Zion English, Patrick Esser, Sumith Kulal, Kyle Lacey, Yam Levi, Cheng Li, Dominik Lorenz, Jonas Müller, Dustin Podell, Robin Rombach, Harry Saini, Axel Sauer, and Luke Smith. Flux.1 kontext: Flow matching for in-context image generation and editing in latent space, 2025. URL `https://arxiv.org/abs/2506.15742`.

Daiqing Li, Aleks Kamko, Ehsan Akhgari, Ali Sabet, Linmiao Xu, and Suhail Doshi. Playground v2.5: Three insights towards enhancing aesthetic quality in text-to-image generation, 2024.

Yumeng Li, Margret Keuper, Dan Zhang, and Anna Khoreva. Divide & bind your attention for improved generative semantic nursing. *arXiv preprint arXiv:2307.10864*, 2023.

Long Lian, Boyi Li, Adam Yala, and Trevor Darrell. Llm-grounded diffusion: Enhancing prompt understanding of text-to-image diffusion models with large language models. *arXiv preprint arXiv:2305.13655*, 2023.

Shanchuan Lin, Bingchen Liu, Jiashi Li, and Xiao Yang. Common diffusion noise schedules and sample steps are flawed. In *Proceedings of the IEEE/CVF winter conference on applications of computer vision*, pp. 5404–5411, 2024.

Tsung-Yi Lin, Michael Maire, Serge Belongie, James Hays, Pietro Perona, Deva Ramanan, Piotr Dollár, and C Lawrence Zitnick. Microsoft coco: Common objects in context. In *European conference on computer vision*, pp. 740–755. Springer, 2014.

Nanye Ma, Shangyuan Tong, Haolin Jia, Hexiang Hu, Yu-Chuan Su, Mingda Zhang, Xuan Yang, Yandong Li, Tommi Jaakkola, Xuhui Jia, et al. Inference-time scaling for diffusion models beyond scaling denoising steps. *arXiv preprint arXiv:2501.09732*, 2025a.

Yuhang Ma, Xiaoshi Wu, Keqiang Sun, and Hongsheng Li. Hpsv3: Towards wide-spectrum human preference score. *arXiv preprint arXiv:2508.03789*, 2025b.

Arash Marioriyad, Mohammadali Banayeeanzade, Reza Abbasi, Mohammad Hossein Rohban, and Mahdieh Soleymani Baghshah. Attention overlap is responsible for the entity missing problem in text-to-image diffusion models!, 2025. URL `https://arxiv.org/abs/2410.20972`.

Viet Nguyen, Anh Nguyen, Trung Dao, Khoi Nguyen, Cuong Pham, Toan Tran, and Anh Tran. Snoopi: Supercharged one-step diffusion distillation with proper guidance, 2024. URL `https://arxiv.org/abs/2412.02687`.

Alex Nichol, Prafulla Dhariwal, Aditya Ramesh, Pranav Shyam, Pamela Mishkin, Bob McGrew, Ilya Sutskever, and Mark Chen. Glide: Towards photorealistic image generation and editing with text-guided diffusion models. *arXiv preprint arXiv:2112.10741*, 2021.

Jonas Oppenlaender. A taxonomy of prompt modifiers for text-to-image generation. *Behaviour & Information Technology*, 43(15):3763–3776, 2024.

William Peebles and Saining Xie. Scalable diffusion models with transformers. In *Proceedings of the IEEE/CVF international conference on computer vision*, pp. 4195–4205, 2023.

Quynh Phung, Songwei Ge, and Jia-Bin Huang. Grounded text-to-image synthesis with attention refocusing. In *Proceedings of the IEEE/CVF Conference on Computer Vision and Pattern Recognition*, pp. 7932–7942, 2024.

Dustin Podell, Zion English, Kyle Lacey, Andreas Blattmann, Tim Dockhorn, Jonas Müller, Joe Penna, and Robin Rombach. Sdxl: Improving latent diffusion models for high-resolution image synthesis. *arXiv preprint arXiv:2307.01952*, 2023.

Alec Radford, Jong Wook Kim, Chris Hallacy, Aditya Ramesh, Gabriel Goh, Sandhini Agarwal, Girish Sastry, Amanda Askell, Pamela Mishkin, Jack Clark, et al. Learning transferable visual models from natural language supervision. In *International conference on machine learning*, pp. 8748–8763. PmLR, 2021.

Colin Raffel, Noam Shazeer, Adam Roberts, Katherine Lee, Sharan Narang, Michael Matena, Yanqi Zhou, Wei Li, and Peter J Liu. Exploring the limits of transfer learning with a unified text-to-text transformer. *Journal of machine learning research*, 21(140):1–67, 2020.

Aditya Ramesh, Prafulla Dhariwal, Alex Nichol, Casey Chu, and Mark Chen. Hierarchical text-conditional image generation with clip latents. *arXiv preprint arXiv:2204.06125*, 1(2):3, 2022.

Royi Rassin, Eran Hirsch, Daniel Glickman, Shauli Ravfogel, Yoav Goldberg, and Gal Chechik. Linguistic binding in diffusion models: Enhancing attribute correspondence through attention map alignment. *Advances in Neural Information Processing Systems*, 36:3536–3559, 2023.

Robin Rombach, Andreas Blattmann, Dominik Lorenz, Patrick Esser, and Björn Ommer. High-resolution image synthesis with latent diffusion models. In *Proceedings of the IEEE/CVF conference on computer vision and pattern recognition*, pp. 10684–10695, 2022.

Olaf Ronneberger, Philipp Fischer, and Thomas Brox. U-net: Convolutional networks for biomedical image segmentation. In *International Conference on Medical image computing and computer-assisted intervention*, pp. 234–241. Springer, 2015.

Seyedmorteza Sadat, Jakob Buhmann, Derek Bradley, Otmar Hilliges, and Romann M Weber. Cads: Unleashing the diversity of diffusion models through condition-annealed sampling. *arXiv preprint arXiv:2310.17347*, 2023.

Seyedmorteza Sadat, Otmar Hilliges, and Romann M Weber. Eliminating oversaturation and artifacts of high guidance scales in diffusion models. In *The Thirteenth International Conference on Learning Representations*, 2024.

Seyedmorteza Sadat, Tobias Vontobel, Farnood Salehi, and Romann M Weber. Guidance in the frequency domain enables high-fidelity sampling at low cfg scales. *arXiv preprint arXiv:2506.19713*, 2025.

Chitwan Saharia, William Chan, Saurabh Saxena, Lala Li, Jay Whang, Emily L Denton, Kamyar Ghasemipour, Raphael Gontijo Lopes, Burcu Karagol Ayan, Tim Salimans, et al. Photorealistic text-to-image diffusion models with deep language understanding. *Advances in neural information processing systems*, 35:36479–36494, 2022.

Axel Sauer, Frederic Boesel, Tim Dockhorn, Andreas Blattmann, Patrick Esser, and Robin Rombach. Fast high-resolution image synthesis with latent adversarial diffusion distillation. In *SIGGRAPH Asia 2024 Conference Papers*, pp. 1–11, 2024a.

Axel Sauer, Dominik Lorenz, Andreas Blattmann, and Robin Rombach. Adversarial diffusion distillation. In *European Conference on Computer Vision*, pp. 87–103. Springer, 2024b.

Hoigi Seo, Junseo Bang, Haechang Lee, Joohoon Lee, Byung Hyun Lee, and Se Young Chun. Geometrical properties of text token embeddings for strong semantic binding in text-to-image generation. *arXiv preprint arXiv:2503.23011*, 2025.

Yang Song, Jascha Sohl-Dickstein, Diederik P Kingma, Abhishek Kumar, Stefano Ermon, and Ben Poole. Score-based generative modeling through stochastic differential equations. *arXiv preprint arXiv:2011.13456*, 2020.

Yang Song, Prafulla Dhariwal, Mark Chen, and Ilya Sutskever. Consistency models. 2023.

Nikita Starodubcev, Denis Kuznedelev, Artem Babenko, and Dmitry Baranchuk. Scale-wise distillation of diffusion models. *arXiv preprint arXiv:2503.16397*, 2025.

Valerii Startsev, Alexander Ustyuzhanin, Alexey Kirillov, Dmitry Baranchuk, and Sergey Kastryulin. Alchemist: Turning public text-to-image data into generative gold. *arXiv preprint arXiv:2505.19297*, 2025.

Ashish Vaswani, Noam Shazeer, Niki Parmar, Jakob Uszkoreit, Llion Jones, Aidan N Gomez, Łukasz Kaiser, and Illia Polosukhin. Attention is all you need. *Advances in neural information processing systems*, 30, 2017.

Bram Wallace, Meihua Dang, Rafael Rafailov, Linqi Zhou, Aaron Lou, Senthil Purushwalkam, Stefano Ermon, Caiming Xiong, Shafiq Joty, and Nikhil Naik. Diffusion model alignment using direct preference optimization. In *Proceedings of the IEEE/CVF Conference on Computer Vision and Pattern Recognition*, pp. 8228–8238, 2024.

Team Wan, Ang Wang, Baole Ai, Bin Wen, Chaojie Mao, Chen-Wei Xie, Di Chen, Feiwu Yu, Haiming Zhao, Jianxiao Yang, et al. Wan: Open and advanced large-scale video generative models. *arXiv preprint arXiv:2503.20314*, 2025.

Xi Wang, Nicolas Dufour, Nefeli Andreou, Marie-Paule Cani, Victoria Fernández Abrevaya, David Picard, and Vicky Kalogeiton. Analysis of classifier-free guidance weight schedulers. *arXiv preprint arXiv:2404.13040*, 2024.

Chenfei Wu, Jiahao Li, Jingren Zhou, Junyang Lin, Kaiyuan Gao, Kun Yan, Sheng-ming Yin, Shuai Bai, Xiao Xu, Yilei Chen, et al. Qwen-image technical report. *arXiv preprint arXiv:2508.02324*, 2025.

Enze Xie, Junsong Chen, Junyu Chen, Han Cai, Haotian Tang, Yujun Lin, Zhekai Zhang, Muyang Li, Ligeng Zhu, Yao Lu, et al. Sana: Efficient high-resolution image synthesis with linear diffusion transformers. *arXiv preprint arXiv:2410.10629*, 2024.

Jiazheng Xu, Xiao Liu, Yuchen Wu, Yuxuan Tong, Qinkai Li, Ming Ding, Jie Tang, and Yuxiao Dong. Imagereward: Learning and evaluating human preferences for text-to-image generation. *Advances in Neural Information Processing Systems*, 36:15903–15935, 2023.

Shai Yehezkel, Omer Dahary, Andrey Voynov, and Daniel Cohen-Or. Navigating with annealing guidance scale in diffusion space. *arXiv preprint arXiv:2506.24108*, 2025.

Sapir Esther Yiflach, Yuval Atzmon, and Gal Chechik. Data-driven loss functions for inference-time optimization in text-to-image generation. *arXiv preprint arXiv:2509.02295*, 2025.

Tianwei Yin, Michaël Gharbi, Taesung Park, Richard Zhang, Eli Shechtman, Fredo Durand, and Bill Freeman. Improved distribution matching distillation for fast image synthesis. *Advances in neural information processing systems*, 37:47455–47487, 2024a.

Tianwei Yin, Qiang Zhang, Richard Zhang, William T Freeman, Fredo Durand, Eli Shechtman, and Xun Huang. From slow bidirectional to fast causal video generators. *arXiv e-prints*, pp. arXiv–2412, 2024b.

Jiahui Yu, Yuanzhong Xu, Jing Yu Koh, Thang Luong, Gunjan Baid, Zirui Wang, Vijay Vasudevan, Alexander Ku, Yinfei Yang, Burcu Karagol Ayan, et al. Scaling autoregressive models for content-rich text-to-image generation. *arXiv preprint arXiv:2206.10789*, 2(3):5, 2022.

Figure 9: We observe that the CLIP text encoder does not influence instruction-guided image editing performed with the FLUX kontext model.

Table 5: Configuration of hyperparameters for dynamic modulation guidance

Task	Positive prompt	Negative prompt	Guidance strategy
Text-to-image `aesthetics`	`Ultra-detailed, photorealistic, cinematic`	`Low-res, flat, cartoonish`	Strategy 1 in Figure 3(b) $i = 5,\ w = 3$
Text-to-image `complexity`	`Extremely complex, the highest quality`	`Very simple, no details at all`	Strategy 1 in Figure 3(b) $i = 10,\ w = 3$
Text-to-image `hands correction`	`Natural and realistic hands`	`Unnatural hands`	Strategy 4 in Figure 3(b) $i_1 = 13, i_2 = 30, i_3 = 45$ $w_1 = 3, w_2 = 1$
Text-to-image `object counting`	[n] [objects]	`Very simple, no details at all`	Strategy 1 in Figure 3(b) $i = 5,\ w = 3$
Text-to-video	`Ultra-detailed, photorealistic, cinematic`	`Low-res, flat, cartoonish`	Strategy 1 in Figure 3(b) $i = 5,\ w = 3$
Image editing	Textual prompt	–	Strategy 1 in Figure 3(b) $i = 5,\ w = 3$

APPENDIX

A ADDITIONAL ANALYSIS FOR FLUX KONTEXT MODEL

Here, we analyze the impact of the CLIP model on FLUX Kontext (Labs et al., 2025). We find that dropping the pooled embedding does not affect editing results, as visually confirmed in Figure 9. In addition, we evaluate performance on the SEED-Data benchmark (Ge et al., 2024) with and without the pooled text embedding. We compute the CLIP score (Hessel et al., 2021) to measure reference preservation and prompt correspondence. The results in Table 6 confirm the observation.

Table 6: Editing quality for the FLUX kontext model (with and without CLIP). CLIP has no effect on the model.

Configuration	CLIP Score, Image ↑	CLIP Score, Text ↑
CLIP+T5	79.3	29.3
w/o CLIP	80 (+0.7)	29.3 (0)

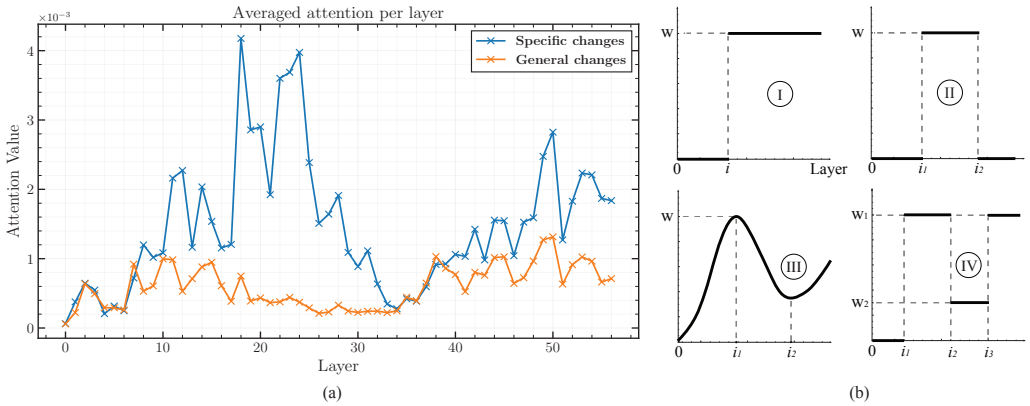

Figure 10: Analysis on dynamic modulation guidance. To derive a dynamic guidance scale, we (a) analyze how the model allocates attention to different features by computing averaged attention maps over two token groups (specific and general). Building on this, we (b) explore dynamic strategies for setting layer-specific w values.

The lack of impact in the editing case may stem from the out-of-distribution nature of instructions for the CLIP model. We find that this mismatch can lead to a lack of editing strength, particularly in complex scenes with multiple objects. To address this, we propose using the final prompt as the CLIP input and applying modulation guidance.

B Strategies for dynamic guidance

Recent studies show that attention layers in transformer models specialize at different depths, with each layer focusing on distinct levels of semantic detail (Avrahami et al., 2025). This insight encourages us to investigate which parts of the attention stack are most appropriate for injecting guidance, depending on the desired effect. For example, if fine-grained attributes such as hands are mainly shaped by mid-layer attention, then targeting guidance at those specific layers is more effective and reduces the risk of unintended modifications in other regions of the image.

Thus, we construct two prompt subsets of $1,000$ examples each: one targeting local features (e.g., `hands`, `face`, `eyes`) and the other targeting global features (e.g., `realism`, `cinematic`, `crisp`). We then generate images for each subset and collect the corresponding attention maps for each target aspect. Finally, we average these maps across all examples and present the results for different layers in Figure 10(a). We observe that the model primarily focuses on local features in two layer regions: layers 10–30 and 42–58. In contrast, attention to global features remains relatively constant, with a slight drop between layers 20 and 35.

Based on this analysis, we propose applying dynamic modulation guidance at the layer level. We present four possible strategies in Figure 10(b), with strategies 3 and 4 designed to resemble the observed attention behavior for specific changes. Interestingly, in Appendix C, we find that these strategies provide better results for `hands correction`. For global changes, the step function (case 1) performs well, outperforming the constant scale. Despite introducing additional hyperparameters, our dynamic guidance offers an extra degree of improvement for practitioners, which we believe is important in real-world applications.

C Ablation study

Dynamic modulation guidance. First, we ablate different dynamic modulation guidance strategies. Specifically, we consider the FLUX schnell model, testing it on the aesthetics, hands correction, and object counting aspects.

We consider different dynamic guidance strategies from Figure 10(b) and compare them to a constant value of $w = 3$. For dynamic strategies, we use the following parameters.

Table 7: Ablation study of dynamic modulation guidance strategies using human preference (side-by-side win rate). The results demonstrate that dynamic guidance outperforms a constant guidance approach.

Configuration		Constant	Strategy 1	Strategy 2	Strategy 3	Strategy 4
`Hands correction`	Original	52	48	49	45	41
	Ours	48 (−4)	52 (+4)	51 (+2)	55 (+10)	59 (+18)
`Object counting`	Original	50	39	40	45	39
	Ours	50 (−0)	61 (+22)	60 (+20)	55 (+10)	61 (+22)
`Aesthetics`	Original	38	28	43	43	46
	Ours	62 (+24)	72 (+44)	57 (+14)	57 (+14)	54 (+8)

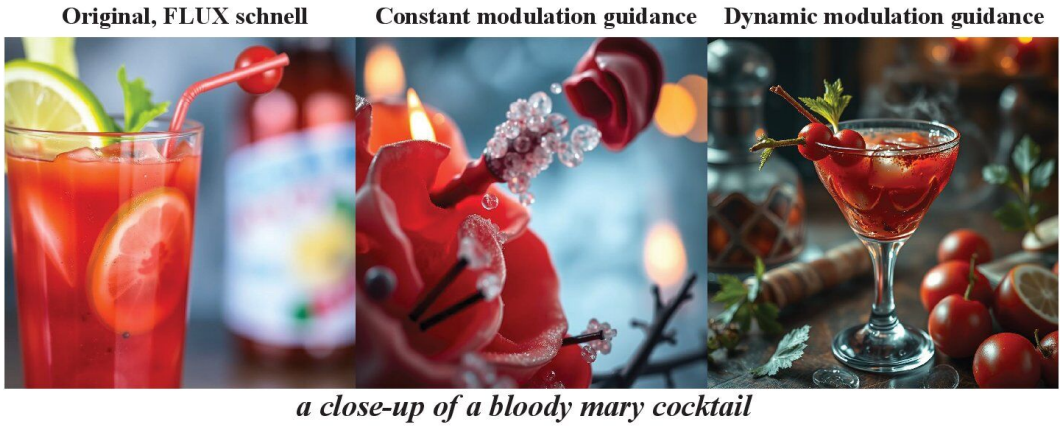

Figure 11: Qualitative comparison of modulation strategies for aesthetics. Constant guidance can overweight the original prompt, leading to significant divergence, whereas dynamic guidance better balances quality and prompt correspondence, allowing the use of larger w without degradation.

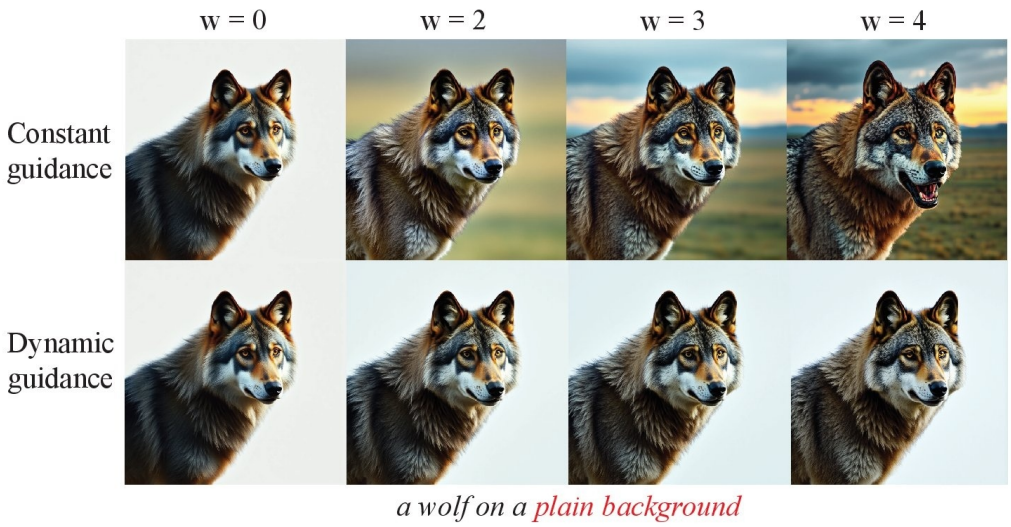

Figure 12: We find that dynamic modulation guidance improves image content (e.g., makes the wolf's fur more detailed) while preserving prompt correspondence. In contrast, constant scales can neglect the prompt request even at small scales (w=2).

Figure 13: Influence of starting layers for complexity guidance. Different choices of i with fixed $w = 3$ illustrate how earlier or later starting layers balance between preserving the original image and improving complexity. In particular, $i = 18$ and $i = 28$ preserve the overall image while enhancing fine-grained details such as faces and hands.

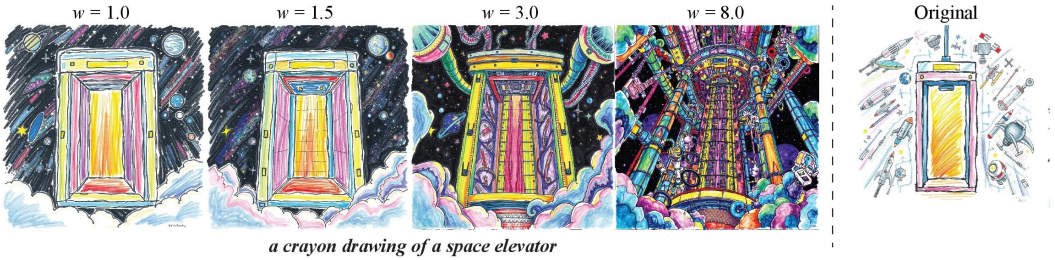

Figure 14: Influence of guidance strength w for aesthetics. With fixed $i = 5$, increasing w improves image quality by boosting the main object (the elevator) and background details. However, excessively large values, such as $w = 8.0$, can introduce artifacts.

- **Strategy 1.** $i = 5, w = 3$;
- **Strategy 2.** $i_1 = 13, i_2 = 30, w = 3$;
- **Strategy 3.** We use two exponential functions with centers at $i_1 = 20, i_2 = 50$, and $w = 3$;
- **Strategy 4.** $i_1 = 13, i_2 = 30, i_3 = 45, w_1 = 3, w_2 = 1$.

Strategies 3 and 4 are designed to follow the attention pattern illustrated in Figure 10(a).

We conduct a human preference study comparing these strategies to the original model, with results presented in Table 7. First, we observe that dynamic strategies yield higher performance gains compared to a constant scale for hands correction and object counting. Moreover, strategy 4 demonstrates the best performance on hands correction, which aligns with the analysis of attention behavior. For object counting, strategies 1 and 4 perform equally well. We therefore select strategy 1 for this aspect due to its simplicity.

Second, for aesthetics guidance, we observe that strategy 1 achieves the best results, while constant guidance also performs well. However, we find that a constant w can introduce artifacts. As shown in Figure 11, constant guidance can overweight the original prompt, causing significant divergence from the source image. In contrast, dynamic guidance achieves a better balance between quality enhancement and prompt correspondence, enabling the use of higher w values without introducing artifacts as shown in Figure 12.

Influence of guidance strength and starting layer number. Next, we analyze how the results change across different starting layers i and modulation guidance strengths w. Our main dynamic strategy is the step function (strategy 1 in Figure 3b), and we ablate different choices for this strategy.

Figure 15: We apply modulation guidance across different CFG values and observe consistent improvements, confirming that it is complementary to CFG.

Specifically, in Figure 13, we evaluate different starting layers i with a fixed $w = 3$ under complexity guidance. This setting allows us to balance original image preservation with complexity improvement. In particular, $i = 18$ and $i = 28$ fully preserve the original image while enhancing only fine-grained details such as face and hands.

Then, in Figure 14, we examine the influence of different w values with a fixed starting layer $i = 5$ under aesthetics guidance. We observe that higher w enhances the main object (e.g., the *elevator* in the example) but also improves background details. However, excessively large values, such as $w = 8$, may introduce artifacts.

Modulation guidance for different CFG. Finally, we examine how modulation guidance behaves under different CFG values, demonstrating that it can operate effectively on top of CFG. Using the FLUX dev model with complexity guidance, we evaluate multiple CFG values in combination with modulation guidance. The results in Figure 15 show that modulation guidance improves performance across different CFG values, confirming that it is complementary to CFG.

D HYPERPARAMETERS CHOICE

In Table 5, we provide the hyperparameters configuration used in our experiments.

For general changes (aesthetics and complexity), we use positive and negative prompts, following the quality-improving prompt modifiers commonly adopted in DMs (Oppenlaender, 2024). In both cases, we employ strategy 1 for dynamic modulation guidance with $w = 3$, but vary the starting layer. Specifically, for complexity, we apply guidance at deeper layers to better preserve the original content while refining high-frequency details.

For specific changes (hands correction and object counting), we adopt strategies 1 and 4, as suggested by the ablation study. For hands correction, we use simple positive and negative prompts: `Natural and realistic hands` and `Unnatural hands`. For object counting, the positive direction

Table 8: Comparison with baselines for **general changes**. We use Normalized Attention Guidance and LLM-enhanced prompts as baselines, and conduct human evaluation on two criteria—**aesthetics** and **complexity**—reporting the corresponding win rates.

Model	Variant	Aesthetics		Complexity	
		Baseline	Variant	Baseline	Variant
Baseline: LLM-enhanced prompts					
FLUX schnell	Ours	45	**55** (+10)	38	**62** (+24)
FLUX schnell	Ours + LLM-enhanced	39	**61** (+22)	26	**74** (+48)
COSMOS	Ours + LLM-enhanced	41	**59** (+18)	35	**65** (+30)
Baseline: Normalized Attention Guidance					
FLUX schnell	Ours	33	**67** (+34)	21	**79** (+58)

Table 9: Comparison with baselines for **specific changes**. We use Concept Sliders and LLM-enhanced prompts as baselines, and conduct human evaluation on two criteria: **defects** for hands correction and **text relevance** for object counting, reporting the corresponding win rates.

Model	Variant	Defects, Hands		Text relevance, Counting	
		Baseline	Variant	Baseline	Variant
Baseline: LLM-enhanced prompts					
FLUX schnell	Ours	26	**74** (+48)	39	**61** (+22)
Baseline: Concept Sliders					
FLUX schnell	Ours	42	**58** (+16)	–	–

is adapted per prompt but follows a general structure: $[n]$[objects], where the main object and desired count are taken from the prompt.

For text-to-video generation, we use the same configuration as in aesthetics guidance for text-to-image generation. We find that this not only makes the videos more realistic but also significantly improves their dynamic degree.

For image editing, we adopt the configuration commonly used in CFG: the original prompt serves as the positive direction and a blank prompt as the negative. This setup increases editing strength in cases where the base FLUX Kontext model struggles. For this setting, we use strategy 1.

E Baselines comparisons for text-to-image generation

We compare our approach against the following baselines: Normalized Attention Guidance (Chen et al., 2025), used for general changes; Concept Sliders (Gandikota et al., 2024), applied to hands correction; and LLM-enhanced prompts (Oppenlaender, 2024), which we consider for both general and specific changes.

For the LLM-enhanced baseline, we use an LLM to modify the prompt sets by adding additional beautifiers, following the same structure used to construct the positive directions in modulation guidance. For the other approaches, we adopt the default configurations provided in their respective papers.

We present the results for **general changes** in Table 8. We observe significant improvements over Normalized Attention Guidance for both criteria (aesthetics and complexity). Importantly, our method does not incur additional overhead, unlike Normalized Attention Guidance, which requires extra passes through computationally intensive attention layers. Second, we find that our approach can be applied on top of LLM-enhanced prompts and brings additional improvements. This is especially important in practice, where different modifiers are commonly applied to basic prompts (Ramesh et al., 2022).

Table 10: Comparison of editing performance measured by VLM scores for **Editing Strength** and **Reference Preservation**.

Configuration	Editing Strength ↑				Reference Preservation ↑			
	Material	Object	Style	Replace object	Material	Object	Style	Replace object
Flux Kontext	66 ±4	78 ±2	68 ±5	71 ±5	93 ±0.1	92 ±0.3	77 ±1	90 ±2
Flux Kontext w/o CLIP	69 (+3)	78 (0)	68 (0)	71 (0)	93 (0)	93 (+1)	79 (+2)	90 (0)
Flux Kontext using final prompt for CLIP	69 (+3)	75 (−3)	68 (0)	73 (+2)	93 (0)	93 (+1)	80 (+3)	89 (−1)
Flux Kontext, modulation guidance	**79** (+13)	**81** (+3)	**72** (+4)	**78** (+7)	93 (0)	92 (0)	78 (+1)	89 (−1)

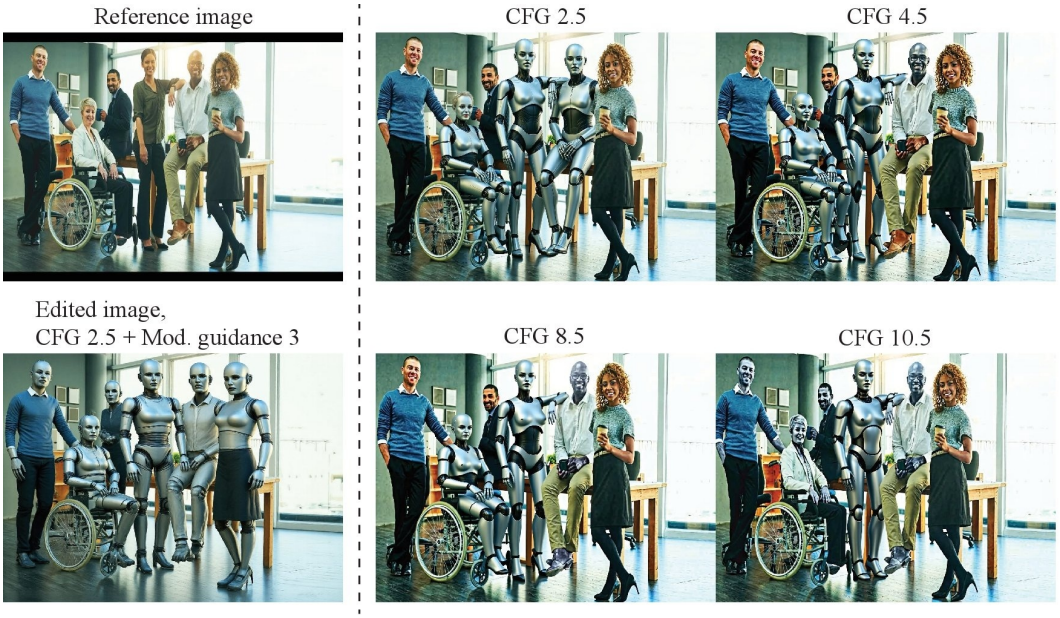

Figure 16: We find that the FLUX Kontext model sometimes struggles with complex image edits, and even higher CFG values do not alleviate this issue. In contrast, modulation guidance can effectively address such cases.

We present the results for **specific changes** in Table 9. First, we find that our approach outperforms the LLM-enhanced prompt baseline on both tasks (hands correction and object counting). Notably, for hands correction, the LLM-enhanced prompt approach can lead to divergence—where the model overemphasizes hands and neglects other parts of the image. In contrast, our approach localizes model attention without adversely affecting the rest of the image. Second, we find that our approach even brings improvements over the Concept Sliders approach, without requiring test-time optimization.

F Instruction-guided image editing

Here, we present the numerical results for instruction-guided image editing using the FLUX Kontext model (Labs et al., 2025). Specifically, we evaluate four settings: (1) the original model; (2) the model without CLIP; (3) the model using the final textual prompt instead of the editing instruction for CLIP; and (4) the model with modulation guidance. For the latter, we use the final prompt as the positive prompt and a blank prompt as the negative, as summarized in Table 5.

To evaluate performance, we follow the basic setting of FLUX Kontext and generate images using the SEED-Data benchmark (Ge et al., 2024), which provides reference images, editing instructions, and final textual prompts. Evaluation is conducted with a VLM model (Bai et al., 2025), which is asked to assess editing strength and reference preservation on a $0 - 100$ scale. For this purpose, we provide the VLM with triples consisting of the reference image, the edited image, and the corresponding instruction.

We report the results in Table 10. First, we observe that removing CLIP does not degrade performance and even yields small improvements, further supporting our intuition that CLIP does not contribute

Table 11: Performance of text-to-image DMs with and without modulation guidance (gray) on Aesthetics and Complexity, evaluated with human preferences and automatic metrics for long and short prompts. Human win rates are reported with respect to the original model; green indicates statistically significant improvement, red a decline. For automatic metrics, **bold** denotes improvement over the original model.

Model	Side-by-Side Win Rate, %				Automatic Metrics, COCO 5k			
	Relevance ↑	Aesthetics ↑	Complexity ↑	Defects ↑	PickScore ↑	CLIP ↑	IR ↑	HPSv3 ↑
FLUX schnell, short prompts					21.6	30.1	6.2	7.8
Ours, Aesthetics guidance	49	**64**	**81**	**57**	**21.9**	**30.2**	**7.4**	**8.5**
FLUX schnell, long prompts					21.0	33.1	10.3	10.8
Ours, Aesthetics guidance	48	**60**	**73**	50	**21.2**	**33.3**	**11.0**	**11.3**

meaningful gains. Second, we find that using the final prompt instead of the editing instruction for the CLIP model leads to inconsistent outcomes—improving material and replacement criteria while degrading performance on object editing. Finally, we observe that modulation guidance consistently provides improvements across all criteria in terms of editing strength.

Specifically, modulation guidance improves performance on complex editing cases, such as those involving multiple objects. As shown in Figure 16, this problem cannot be solved by simply increasing the CFG scale—only modulation guidance provides improvements.

G Additional experiments

Additionally, we report experimental results for long and short prompts separately to demonstrate that our approach works well with long prompts, whereas basic CLIP tends to influence only short prompts. We conduct a quantitative evaluation using prompts from the MJHQ dataset separated into long and short prompts. We calculate automatic metrics using $1,000$ prompts and conducted a human evaluation using 300 prompts. The results are presented in Table 11. We find that our modulation guidance also has a positive impact on long prompts. For instance, human evaluation shows improvements of $+20\%$ in aesthetics and $+46\%$ in image complexity compared to the original model (FLUX schnell).

H Limitations

Our approach also has several limitations. First, it does not address text-to-image correspondence, meaning that it cannot improve how accurately the generated image reflects the input prompt. This limitation is inherent to the modulation guidance design, which focuses on enhancing aesthetic quality, complexity, and other visual attributes rather than semantic alignment. Second, our method introduces a small number of additional hyperparameters that must be tuned to achieve optimal performance. While this tuning process is relatively straightforward, it may add an extra step compared to baseline methods that do not require such configuration.

I More visual results

We provide additional visual comparisons in Figures 17, 18, 19, 20, 21, 22, and 23.

J Human evaluation

The evaluation is conducted using Side-by-Side (SbS) comparisons, where assessors are presented with two images alongside a textual prompt and asked to choose the preferred one. For each pair, three independent responses are collected, and the final decision is determined through majority voting.

The human evaluation is carried out by professional assessors who are formally hired, compensated with competitive salaries, and fully informed about potential risks. Each assessor undergoes detailed training and testing, including fine-grained instructions for every evaluation aspect, before participating in the main tasks.

In our human preference study, we compare the models across four key criteria: relevance to the textual prompt, presence of defects, image aesthetics, and image complexity. Figures 24, 27, 25, 26 illustrate the interface used for each criterion. Note that the images displayed in the figures are randomly selected for demonstration purposes.

K ADDITIONAL DISCUSSION

This work involves human evaluations conducted through side-by-side image comparisons to assess model performance across various criteria (e.g., aesthetics, complexity, and defects). All human studies were performed with informed consent, and participants were compensated fairly for their time. No personally identifiable information was collected, and all data were anonymized prior to analysis. Our research uses publicly available datasets and pre-trained models, adhering to their respective licenses and terms of use. While our method aims to improve the quality and controllability of generative models, we recognize the potential for misuse of generative technologies, including the creation of misleading or harmful content. We encourage responsible use and recommend implementing safeguards in real-world applications.

We note that in this paper a large language model (LLM) was used exclusively for polishing the writing. It was not employed to generate ideas, methods, or contributions.

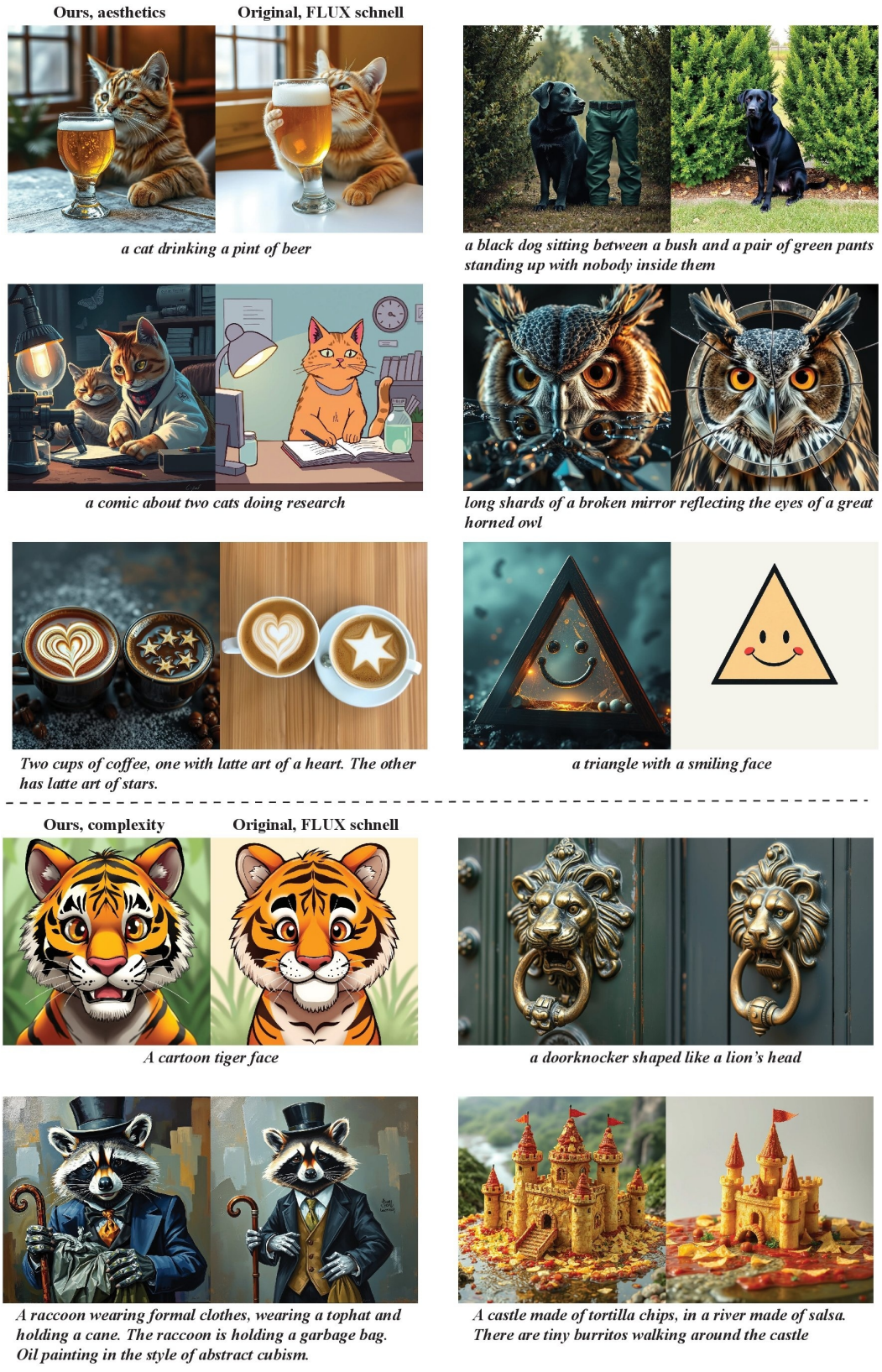

Figure 17: Visual comparisons for FLUX schnell model

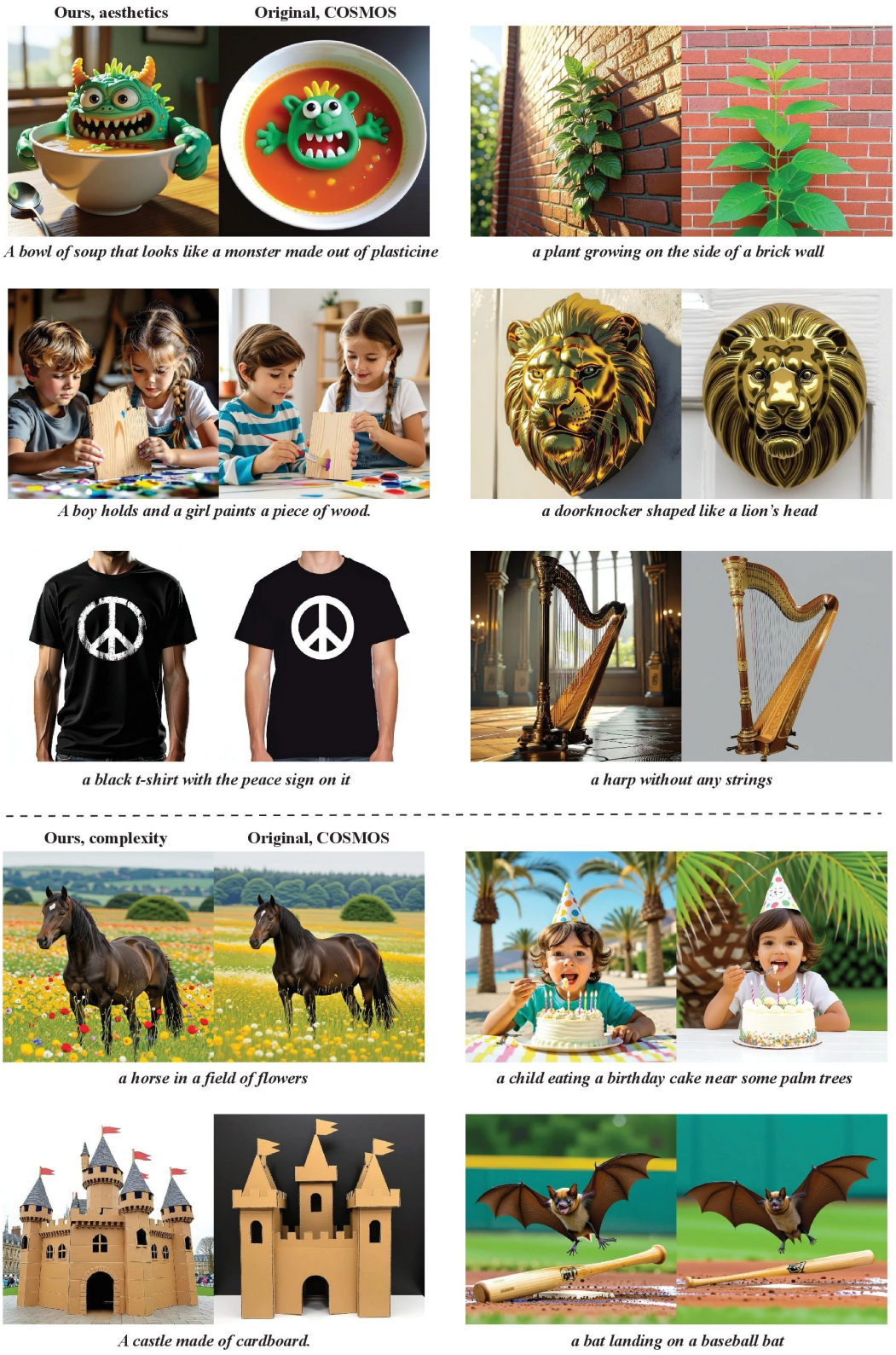

Figure 18: Visual comparisons for COSMOS model

Figure 19: Visual comparisons for HiDream-Fast model

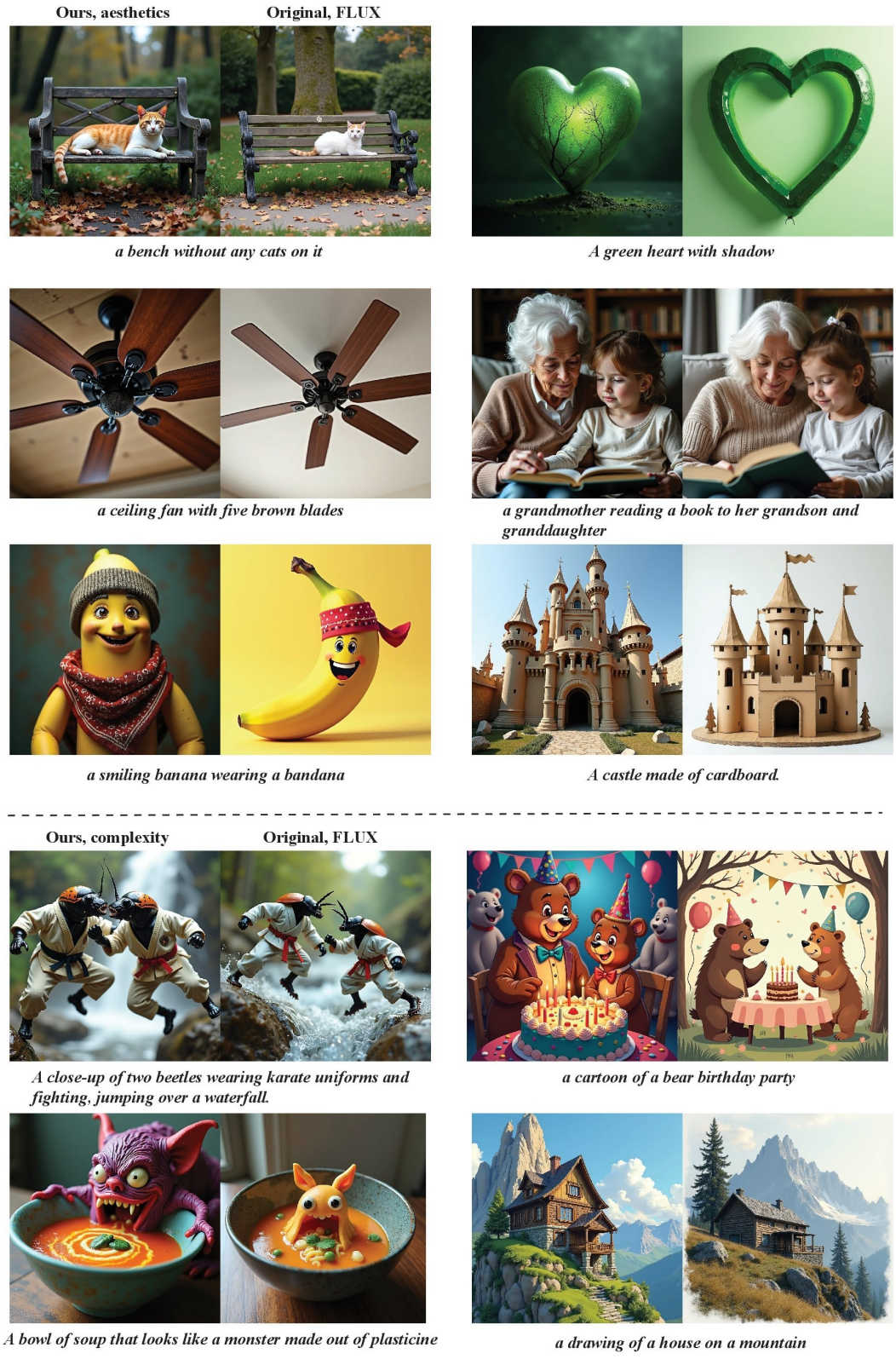

Figure 20: Visual comparisons for FLUX model

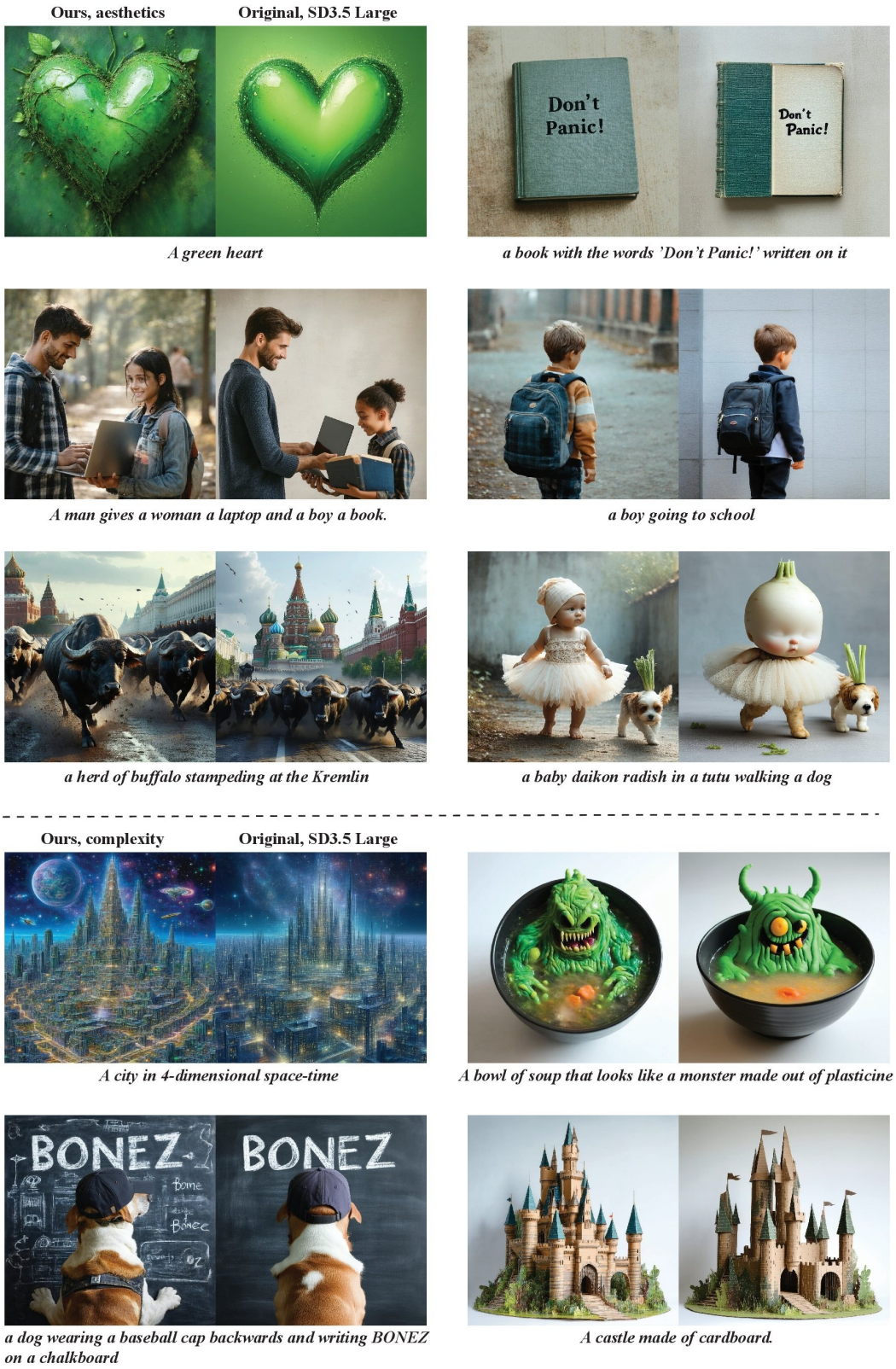

Figure 21: Visual comparisons for SD3.5 Large model

Figure 22: Visual comparisons for FLUX schnell model

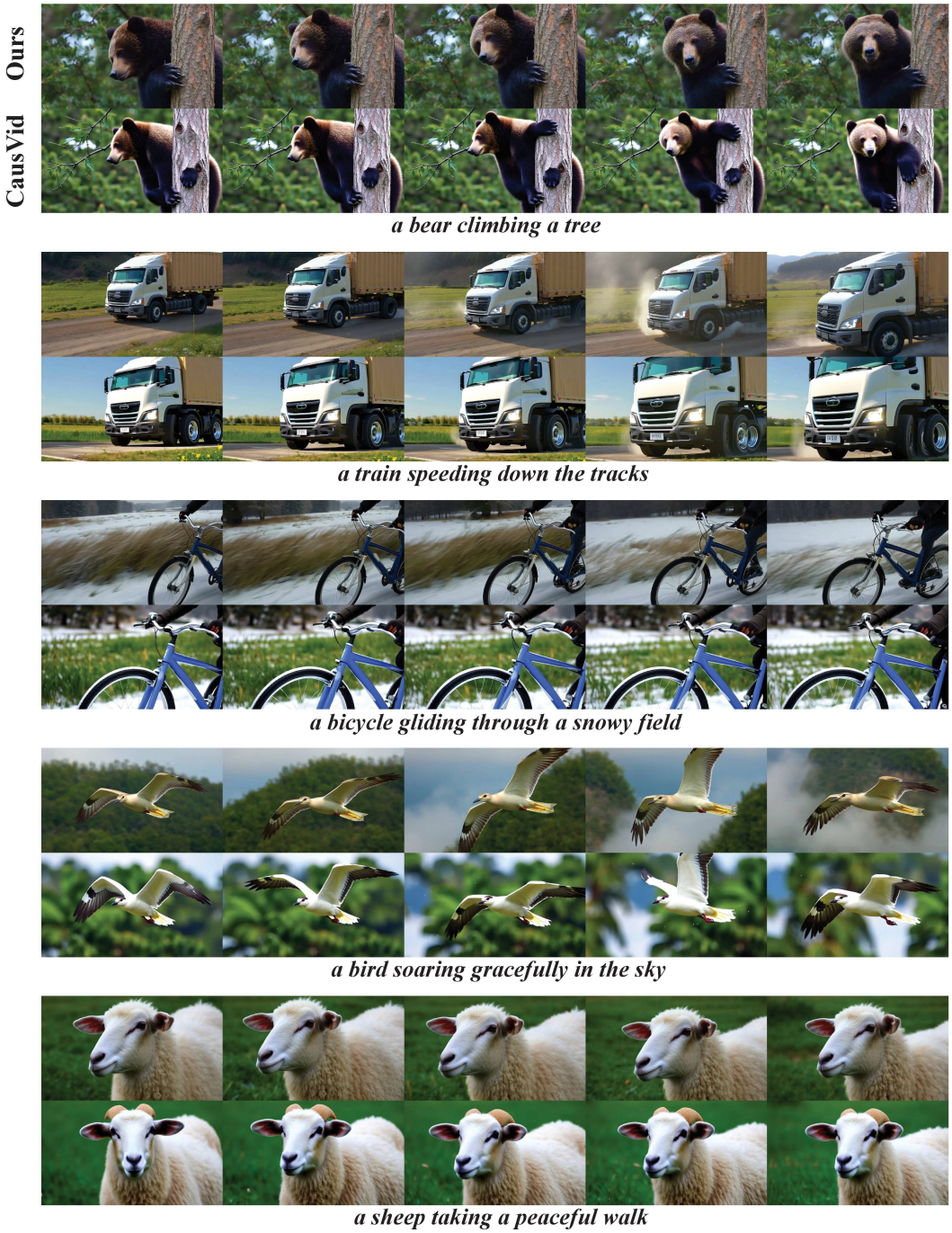

Figure 23: Visual comparisons for CausVid video model

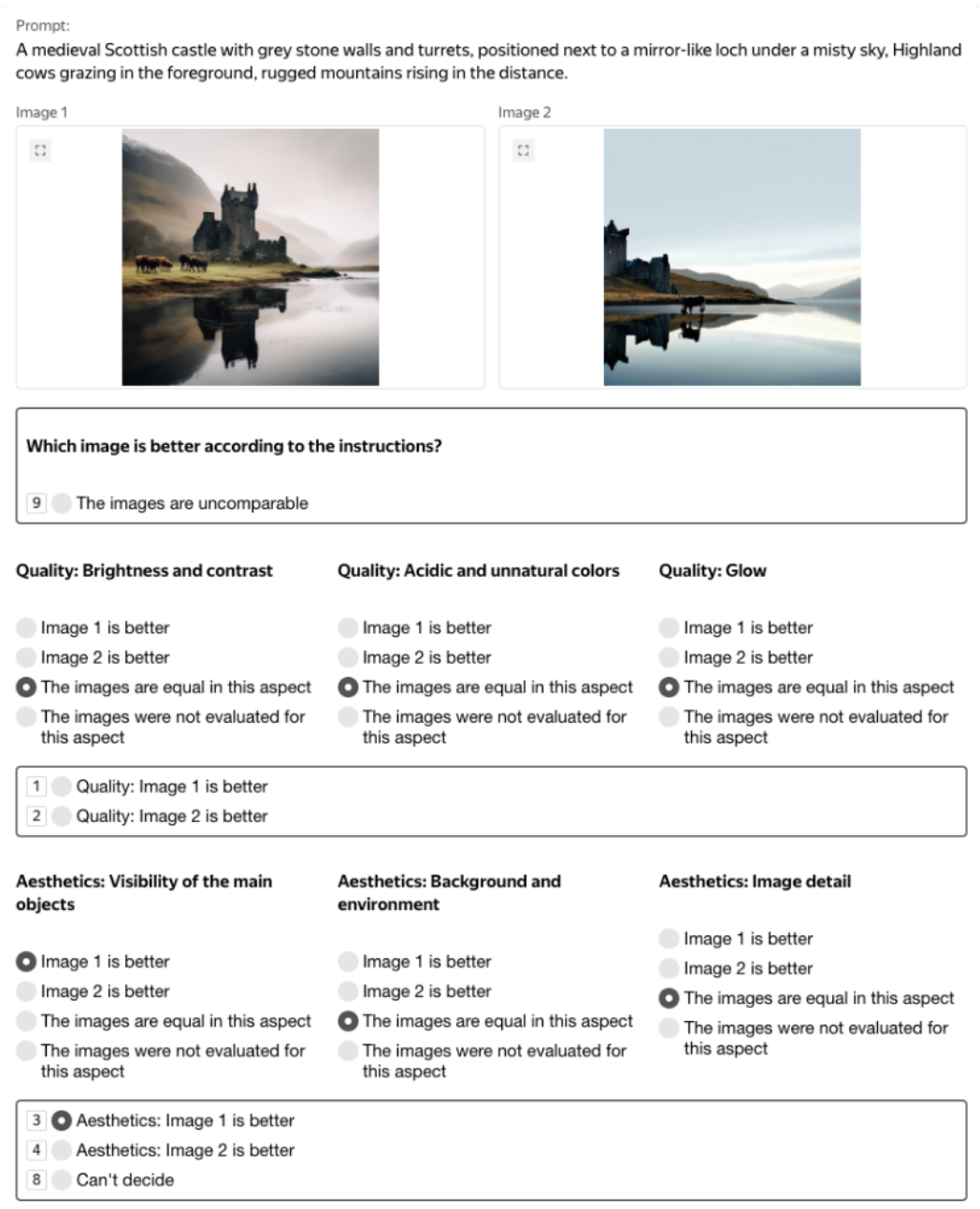

Figure 24: Human evaluation interface for aesthetics.

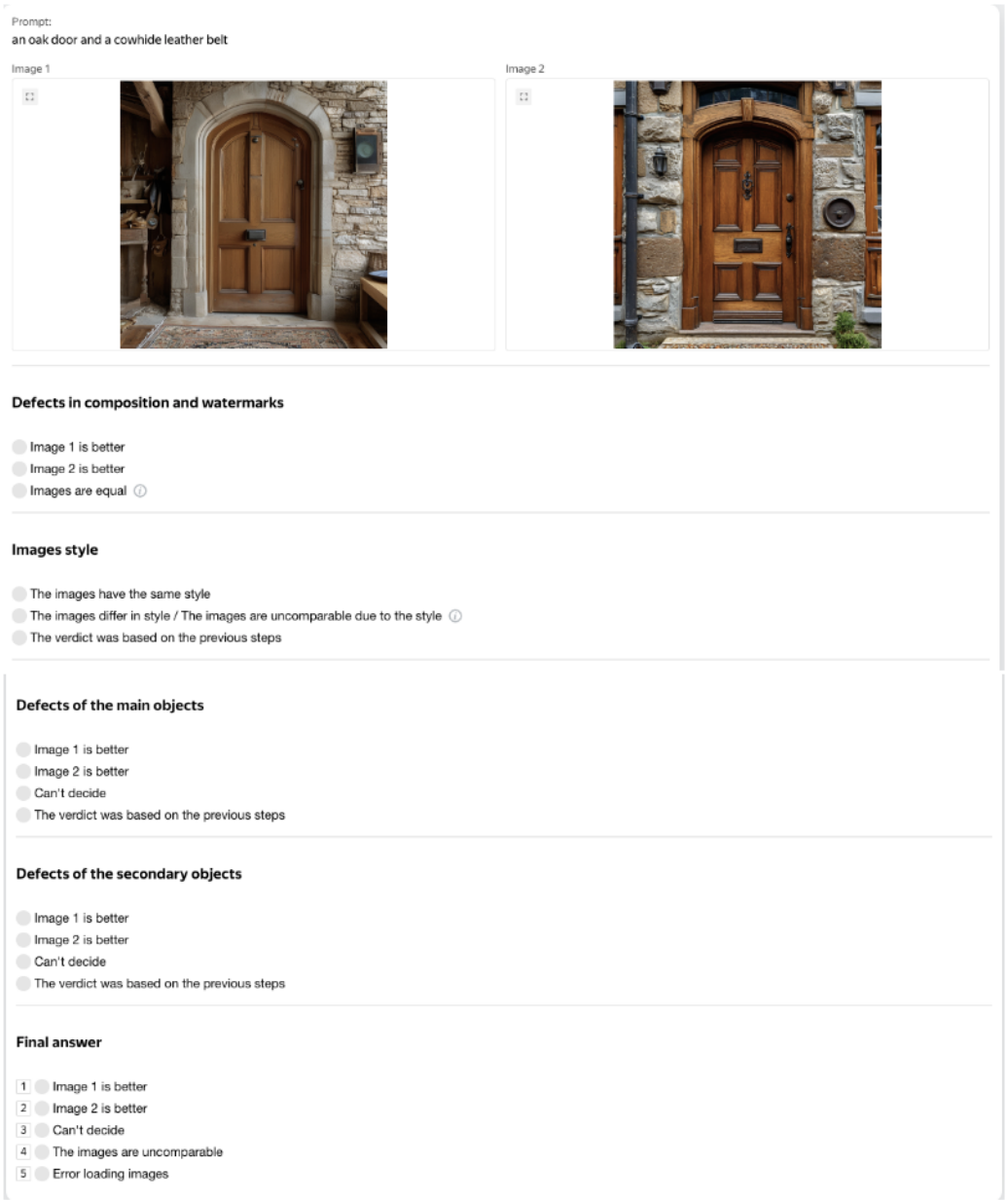

Figure 25: Human evaluation interface for defects.

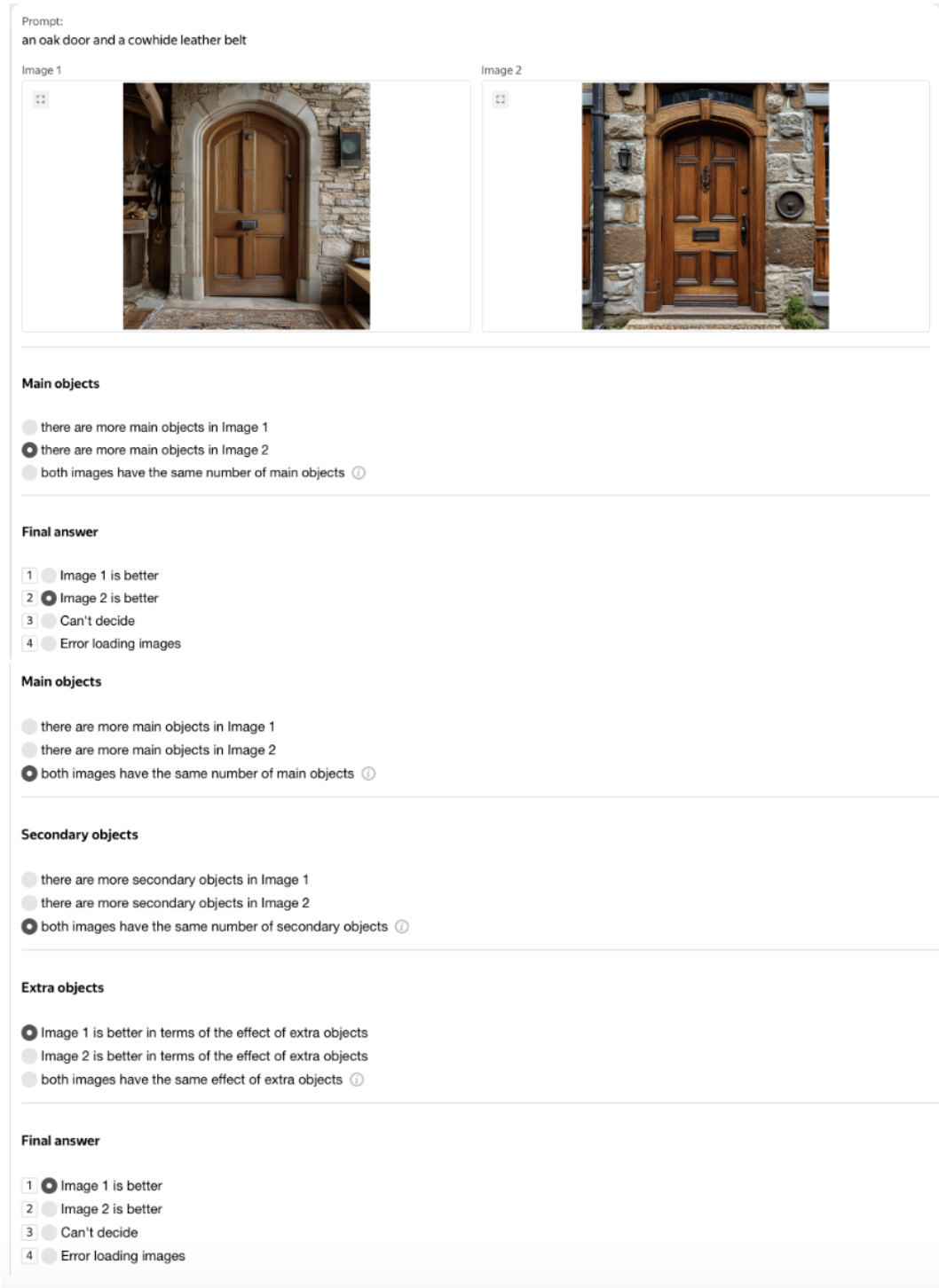

Figure 26: Human evaluation interface for relevance.

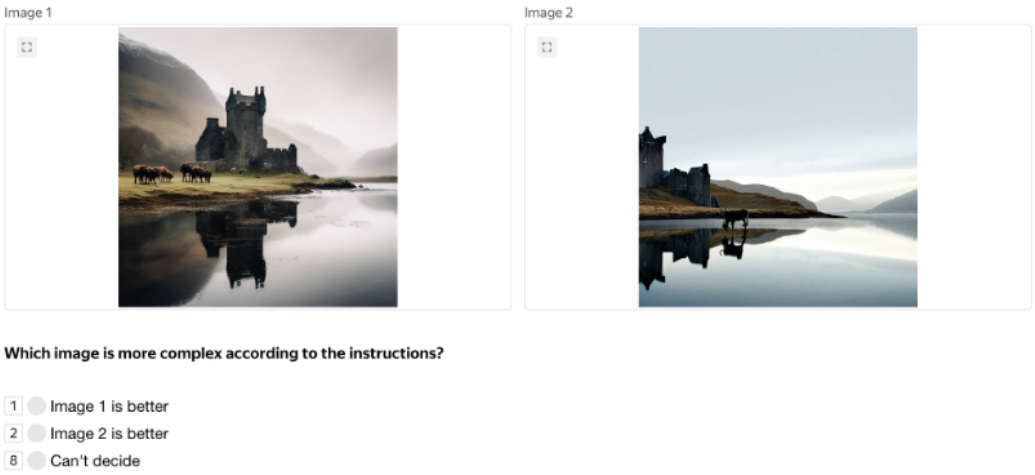

Figure 27: Human evaluation interface for complexity.